Core Collapse in Rotating Massive Stars and the Production of GRBs

Aldo Batta

Instituto de Astronomía UNAM, México
William Lee

Nikko Japan, IAU Symposium 279

Main Objectives & Considerations

Study effects of self gravity and cooling on the overall morphology and evolution of the accretion flow (in 3D) in the context of the collapsar model.

- Fixed rotation rate
- Polytropic envelope $\gamma = 5/3$ (simple EOS)
- Accretion onto a black hole (BH) (pseudo-Newtonian approximation)
- Simplified cooling prescription to explore different cooling efficiencies
- GADGET-2 (Volker 2005)

Accretion and GRBs. The Collapsar Model

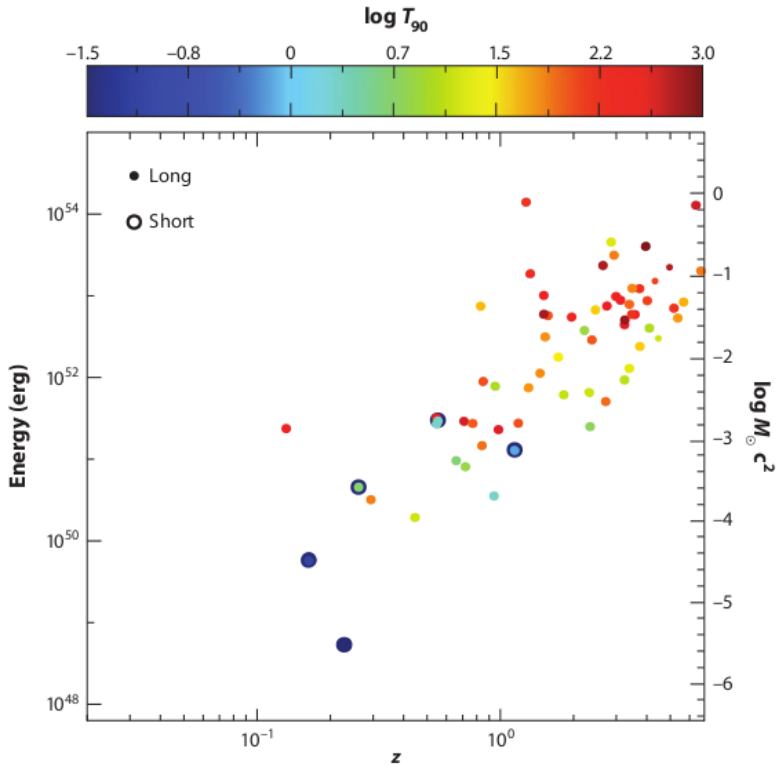

Figure 2

Apparent isotropic γ-ray energy as a function of redshift and observed duration. The energy is calculated assuming isotropic emission in a common comoving bandpass for a sample of short and long GRBs with measured redshifts. This spread in the inferred luminosities obtained under the assumption of isotropic emission may be reduced if most GRB outflows are jet-like. A beamed jet would alleviate the energy requirements, and some observational evidence does suggest the presence of a jet.

(from Gehrels et al. 2009)

GRBs energies exceed $10^{53}(\Omega/4\pi)$ ergs.

- Spectral energy distributions peaking at γ rays.
- Long GRB can be associated with a SN (with no H lines)
- Massive enough to form a BH from its Fe core
- Without H envelope
- Rotating fast enough to produce a disk around the BH.

The Collapsar Model

EOS and cooling/heating mechanisms

Temperatures and densities estimated near the BH can reach: $\rho \simeq 10^{11}$ g cm^{-3}, $T \simeq 10^{11}$ K

- Pair creation $\rightarrow$ electron-positron pressure $P_{e^\pm}$
- Black body radiation pressure (trapped photons)
- Free nucleons and α particles ideal gas
- Neutrino cooling (pair anihilation, neutronization, ...)

  Estimate $t_\nu \rightarrow$ for T and ρ expected.
  non-degenerate relativistic $e^\pm$, and
  ionized H ideal gas
  cooled by e^- capture and pair anihilation

Neutrino Cooling Timescale

$$u = \frac{3}{2}\frac{kT\rho}{\mu m_p} + \frac{11}{4}aT^4$$

$$q_\nu \simeq 5 \times 10^{33} T_{11}^9 + 9.0 \times 10^{23} \rho T_{11}^6$$

(Narayan et al. 2001)

$$t_\nu = u/q_\nu$$

The Collapsar Model

EOS and cooling/heating mechanisms

Temperatures and densities estimated near the BH can reach: $\rho \simeq 10^{11}$ g cm^{-3}, $T \simeq 10^{11}$ K

- Pair creation $\rightarrow$ electron-positron pressure $P_{e^\pm}$
- Black body radiation pressure (trapped photons)
- Free nucleons and α particles ideal gas
- Neutrino cooling (pair anihilation, neutronization, ...)

  Estimate $t_\nu \rightarrow$ for T and ρ expected.
  non-degenerate relativistic $e^\pm$, and
  ionized H ideal gas
  cooled by e^- capture and pair anihilation

Neutrino Cooling Timescale

$$u = \frac{3}{2}\frac{kT\rho}{\mu m_p} + \frac{11}{4}aT^4$$

$$q_\nu \simeq 5 \times 10^{33} T_{11}^9 + 9.0 \times 10^{23} \rho T_{11}^6$$

(Narayan et al. 2001)

$$t_\nu = u/q_\nu$$

The Collapsar Model

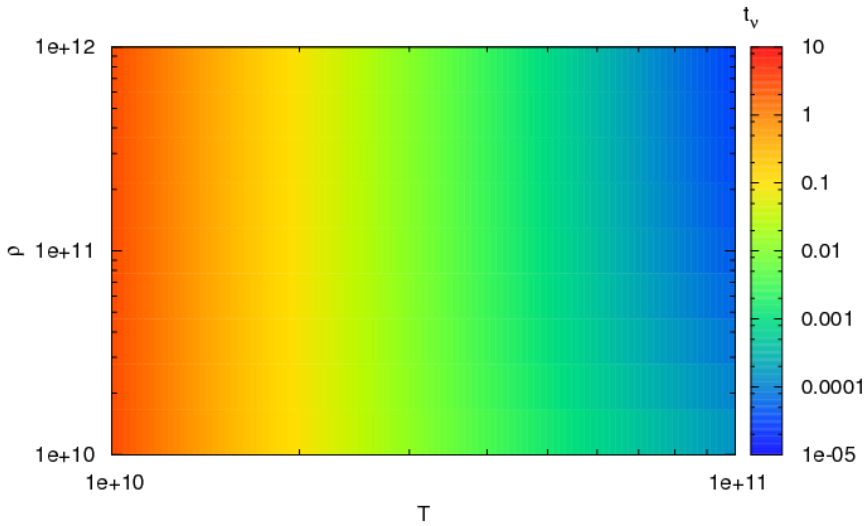

Fig. 5 Neutrino Cooling timescale obtained from assuming an ideal gas, radiation pressure and non-degenerate relativistic electrons and positrons.

Neutrino Cooling Timescale

$$u = \frac{3}{2}\frac{kT\rho}{\mu m_p} + \frac{11}{4}aT^4$$

$$q_\nu \simeq 5 \times 10^{33} T_{11}^9 + 9.0 \times 10^{23} \rho T_{11}^6$$

$$t_\nu = u/q_\nu$$

Cooling prescription

$$t_{cool} = \beta t_{disk} \qquad \rightarrow \frac{du}{dt} = -\frac{u}{t_{cool}}$$

Gas orbits the BH $\sim \beta$ times before cooling down.

The Collapsar Model

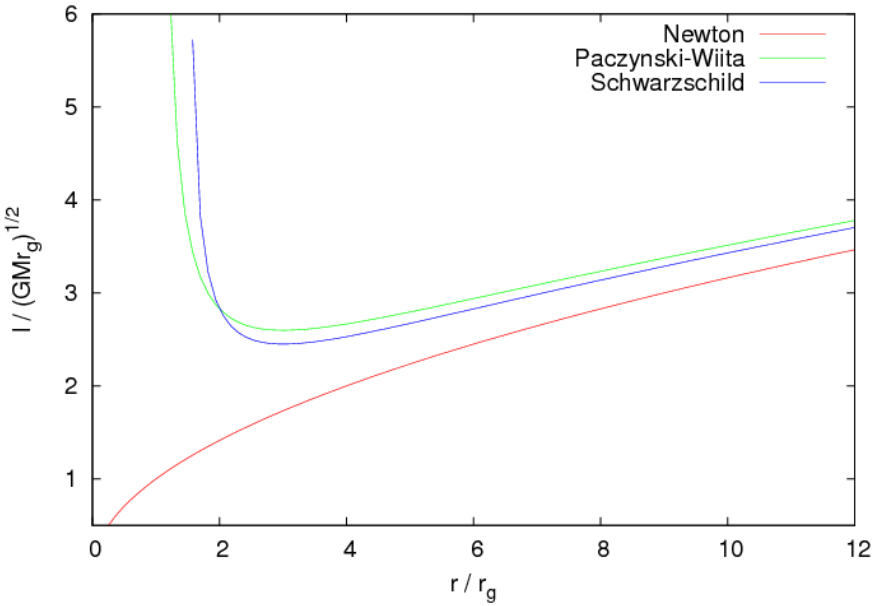

Fig. 6 Keplerian angular momentum distribution for a test particle in a Newtonian (red line), a Paczynski-Wiita (green line) and a Schwarzschild BH potential (blue line).

Angular Momentum Distribution

Minimum angular momentum determined by the innermost stable circular orbit (ISCO) $R_{isco} = 3r_g$ and gas velocity $\sim c$

$$J_{min} = R_{isco} c$$
$$= \frac{6GM_{AN}}{c} \sim 10^{16} \, (M/M_\odot) \, \mathrm{cm^2 s^{-1}}$$

Paczynski-Wiita (PW) potential $\rightarrow R_{isco}$

$$\Phi = -\frac{GM}{r - r_g}$$

$J > J_{min}$ (but below breakup)

Material at $r \leq 3r_g$ is considered accreted

The Collapsar Model

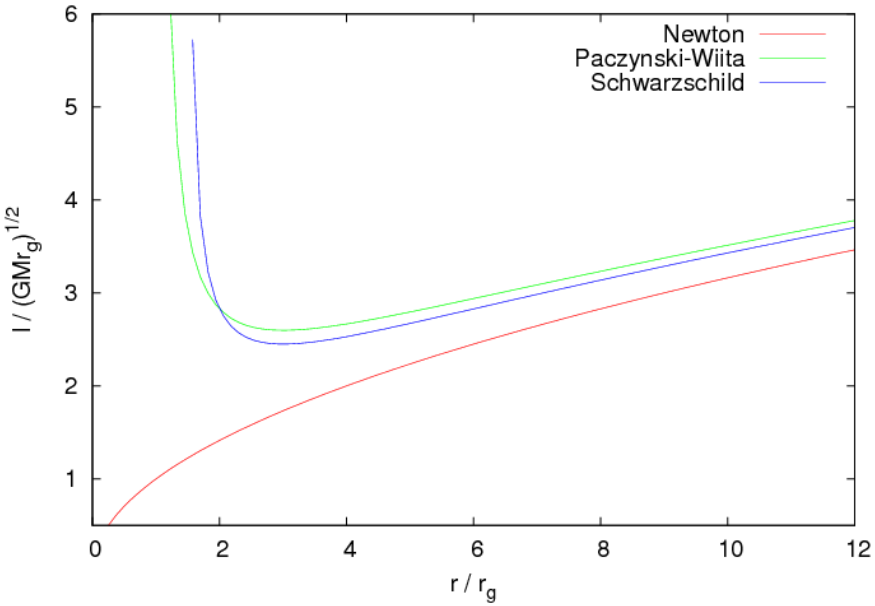

Fig. 6 Keplerian angular momentum distribution for a test particle in a Newtonian (red line), a Paczynski-Wiita (green line) and a Schwarzschild BH potential (blue line).

Angular Momentum Distribution

Minimum angular momentum determined by the innermost stable circular orbit (ISCO) $R_{isco} = 3r_g$ and gas velocity $\sim c$

$$J_{min} = R_{isco} c$$
$$= \frac{6GM_{AN}}{c} \sim 10^{16} \, (M/M_\odot) \, \mathrm{cm^2 s^{-1}}$$

Paczynski-Wiita (PW) potential $\rightarrow R_{isco}$

$$\Phi = -\frac{GM}{r - r_g}$$

$J > J_{min}$ (but below breakup)

Material at $r \leq 3r_g$ is considered accreted

Cooling and Instabilities in Collapsed Rotating Cores

Towards a Collapsar Model

$4.5M_\odot$ Polytropic stars, whose $2M_\odot$ innermost mass is collapsed into a BH

Rigid body rotation (below breakup)

- BH cannot move
- Different cooling efficiencies from Adiabatic ($\Gamma = 5/3$) to isothermal ($\Gamma \simeq 1$)
- Cooling prescription $du/dt = -u/t_{cool}$

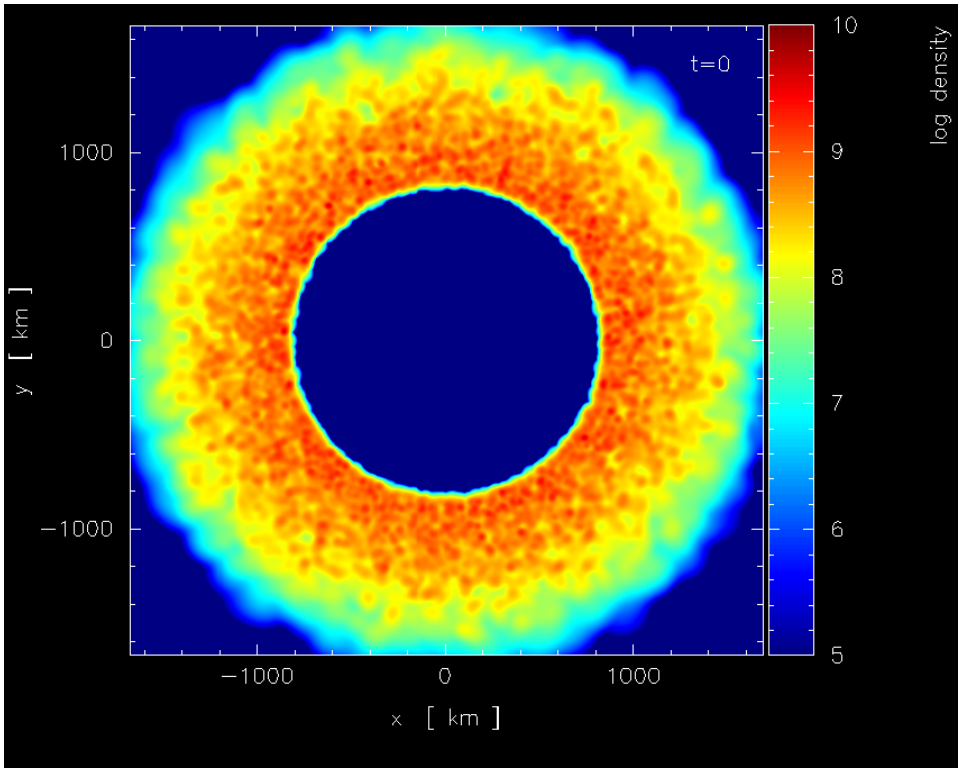

Fig. 10 Density at the XY plane for the $4.5M_\odot$ polytropic star with its innnermost $2M_\odot$ turned into a BH.

Cooling and Instabilities in Collapsed Rotating Cores

Cooling schemes

Model	Cooling efficiency β	t_{cool}
βAd	Adiabatic	–
β13.2	13.243	1.2319 s
β2.6	2.6487	0.24639 s
β1.3	1.3243	0.12319 s
β0.26	0.26487	0.024639 s
β0.026	0.026487	0.0024639 s
βIso	Isothermal	–

Table 1. Cooling times t_{cool} and efficiency parameters β used on our simulations. All times range on the neutrino cooling time t_ν previously estimated.

Cooling efficiency $\beta \rightarrow t_{cool} = \beta t_{disk}$
$t_{disk} = 0.093$ s

Gas orbits the BH $\sim \beta$ times before cooling down.

Accretion Rates and BH Mass

- Slowly cooled envelopes show smooth increase in accreted mass (at least for a while).
- Increasing cooling efficiency $\rightarrow$ accreted mass & accretion rates increases

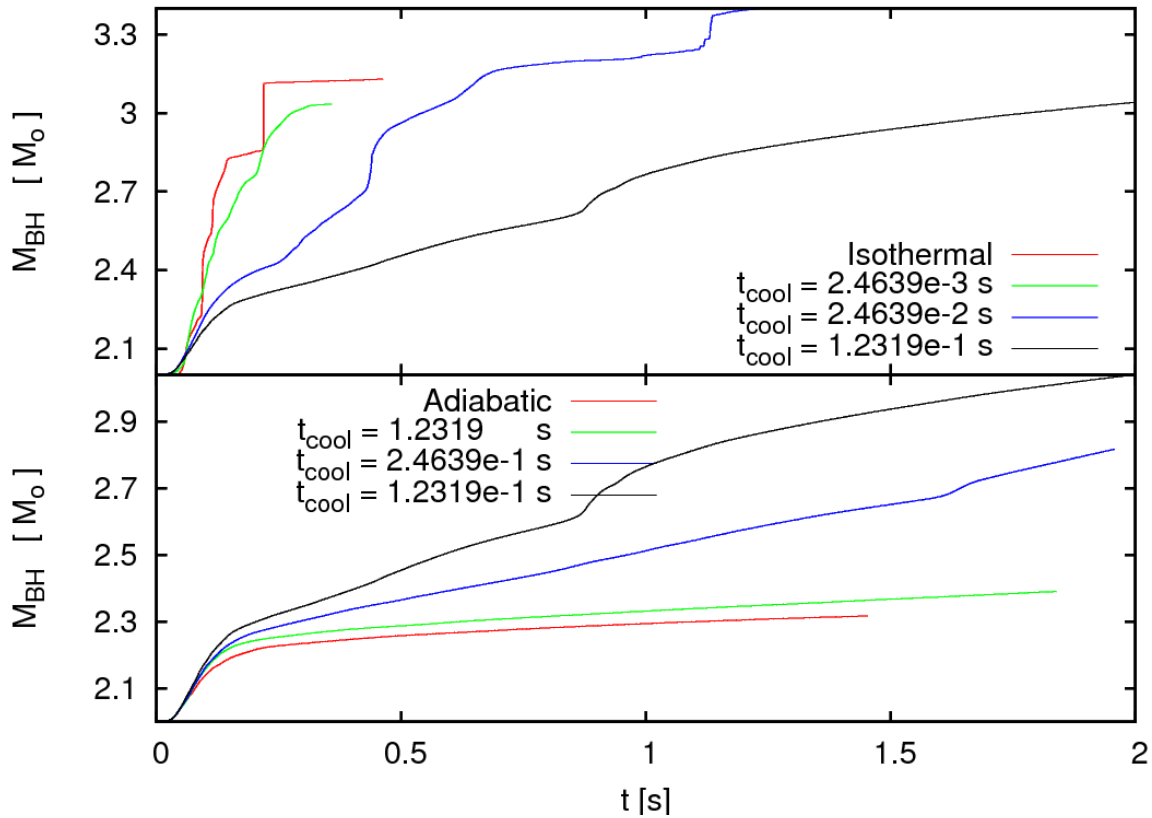

Fig. 13 BH mass (solar masses) as function of time (seconds) for different cooling schemes used. At the top panel we show the envelopes with the smaller cooling time scale t_{cool} which resemble the most to the isothermal envelope (red line). On the bottom panel we show the slowly cooled envelopes which resemble the most to the adiabatic envelope (red line).

Accretion Rates and BH Mass

- Slowly cooled envelopes show few or none strong variations in $\dot{M}$
- Increasing cooling efficiency $\rightarrow$ accretion rates & its variations increase

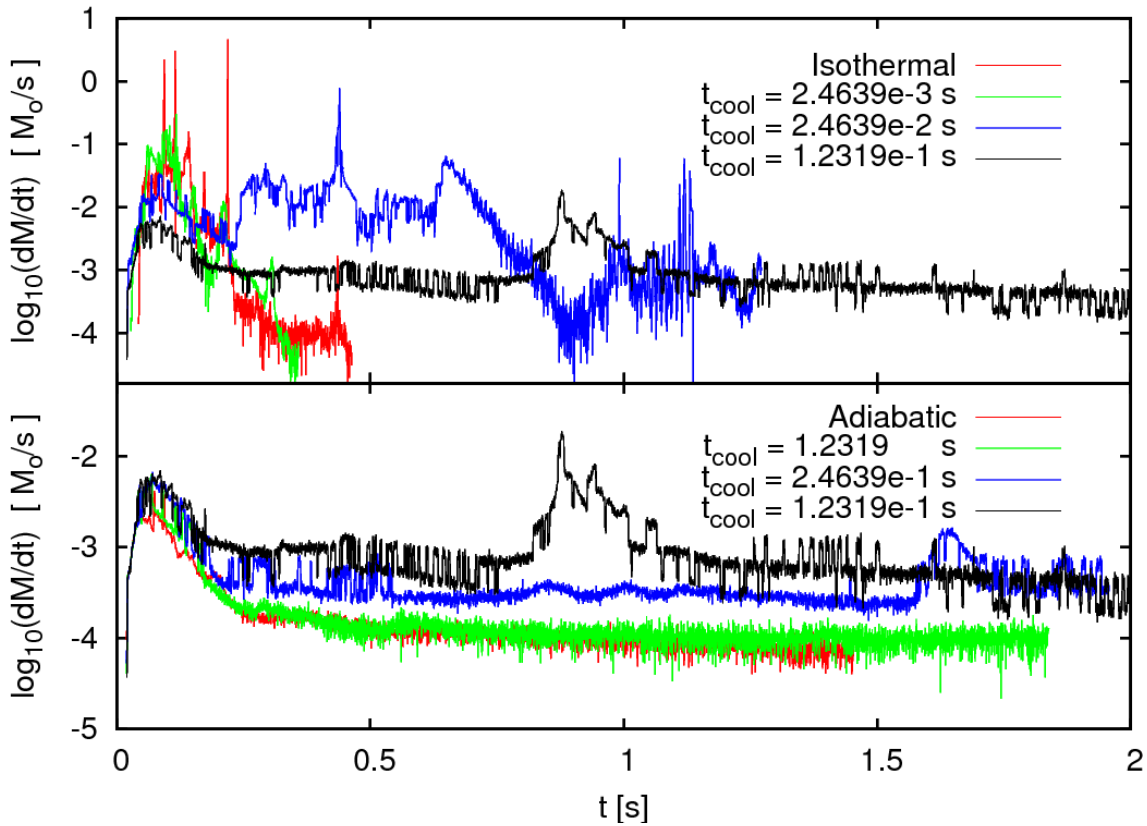

Fig. 14 Logarithm of the BH accretion mass rate $\dot{M}$ in solar masses per second. At the top panel we show the envelopes with the smaller cooling time scale t_{cool} which resemble the most to the isothermal envelope (red line). On the bottom panel we show the slowly cooled envelopes which resemble the most to the adiabatic envelope (red line).

Energy Loss Rates

- Each fluid element (SPH particle) loses $du_i/dt = u_i/t_{cool}$
- Total energy loss rate $L_c = \sum m_i(du_i/dt)$ and energy lost $u_c = \int L_c dt$

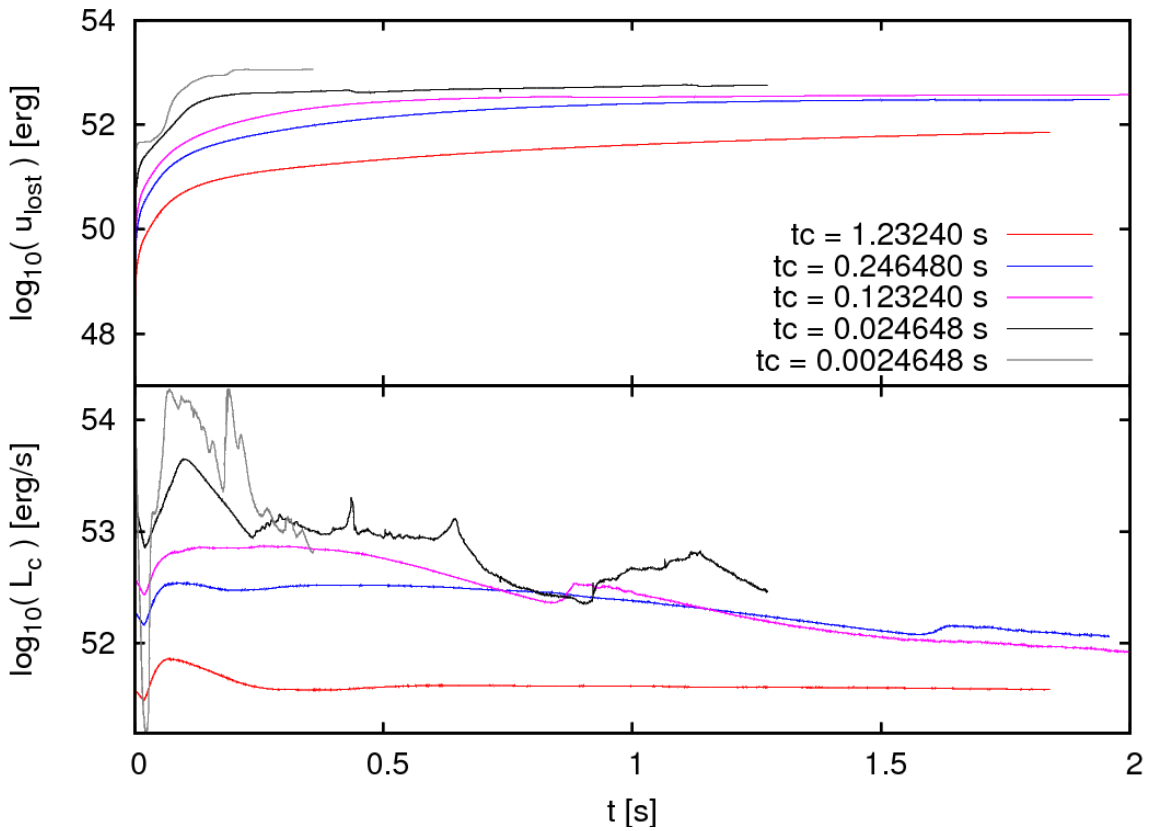

Fig. 15 Logarithm of the energy loss rate L_c (bottom panel) in erg/s for models $\beta 13.2$ (red line), $\beta 2.6$ (blue line), $\beta 1.3$ (pink line), $\beta 0.26$ (orange line) and $\beta 0.026$ (gray line). At the top panel we show the sum of the energy lost by all SPH particles u_{lost} as a function of time.

Energy Loss Rates

- Each fluid element (SPH particle) loses $du_i/dt = u_i/t_{cool}$
- Total energy loss rate $L_c = \sum m_i(du_i/dt)$ and energy lost $u_c = \int L_c dt$

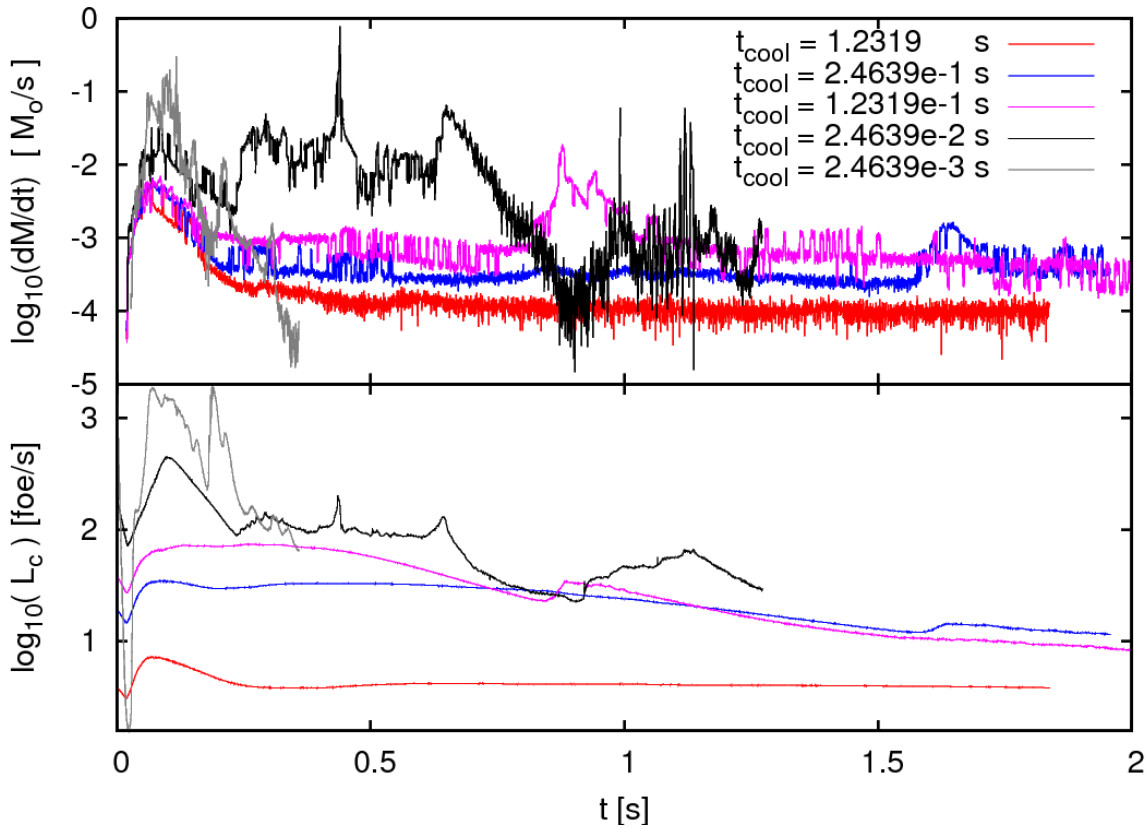

Fig. 15 Logarithm of the energy loss rate L_c (bottom panel) in erg/s for models $\beta 13.2$ (red line), $\beta 2.6$ (blue line), $\beta 1.3$ (pink line), $\beta 0.26$ (orange line) and $\beta 0.026$ (gray line). At the top panel we show the sum of the energy lost by all SPH particles u_{lost} as a function of time.

Morphological Features

Characterize non-axisymmetric instabilities $\rightarrow$ Fourier transform (FT) on the azimuthal distribution of mass $\Phi_M = \int \left[\int \rho(\phi, r, z) dz\right] r\, dr$ as in (Zurek & Benz, 1986), we define the amplitude of the m mode by:

$$C_m = \frac{1}{2\pi} \int_0^{2\pi} e^{im\phi} \Phi_M d\phi$$

Relative power $|c_m|^2 = |C_m|^2/|C_0|^2$ indicates the intensity of m spiral arms compared to the disk integrated mass. Which should be visible on density maps.
Check for unstable regions at the disk $\rightarrow$ Toomre parameter

$$Q_T = \frac{\kappa c_s}{\pi G \Sigma}$$

where $\kappa = (\partial W/\partial r)^{1/2}$ is the epicyclic frequency obtained from first order perturbations in the disk material subject to the effective potential $W(r) = \phi(r) + l^2/2r^2$, $\Sigma(r, \phi)$ is the superficial density of the disk and c_s is the local sound speed.

$\beta 2.6$ Model, $t_{cool} = 0.246$ s

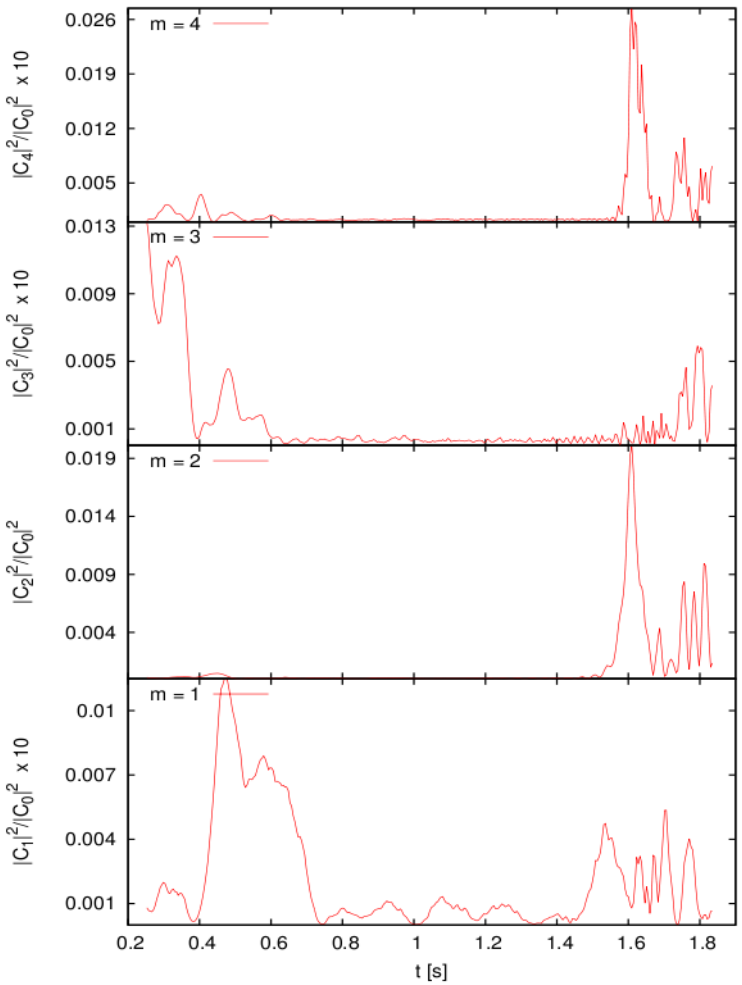

Fig. 18 Relative power $|c_m|^2 = |C_m|^2/|C_0|^2$ ($m = 1, 2, 3, 4$) for the azimuthal's distribution of mass Φ_M Fourier transform of $\beta 2.6$ model ($|c_m|^2$ values are scaled for modes $m = 1$, 3 and 4).

- Intense variations on $\dot{M}$ and L_c happen at the same time.
- The relative power $|c_2|^2$ has an intense peak ($\gtrsim 10$ times) at $t = 1.6$ where intense variations on $\dot{M}$ and L_c start.
- Intense structure formation $\rightarrow$ variations on L_c and $\dot{M}$

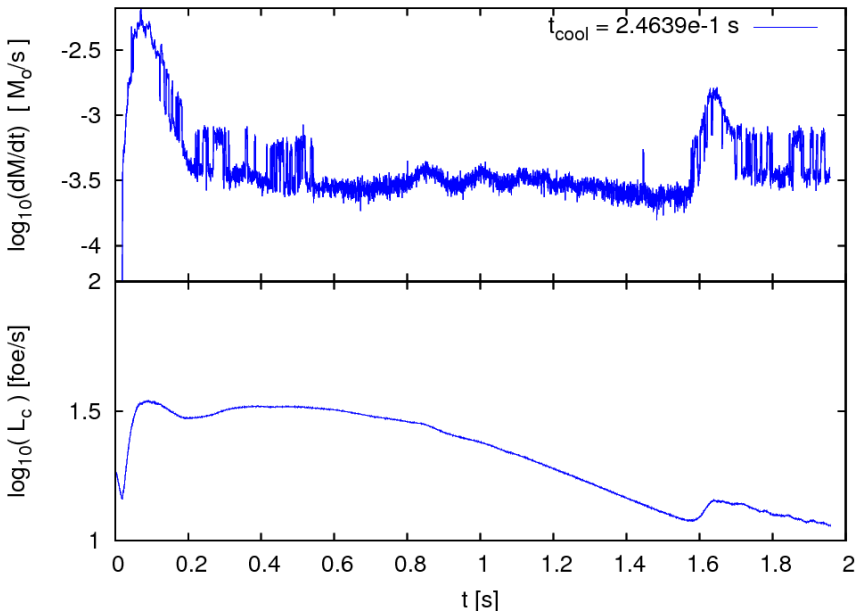

Fig. 19 Mass accretion and energy loss rates (top panel and bottom panel respectively).

$\beta 2.6$ Model, $t_{cool} = 0.246$ s

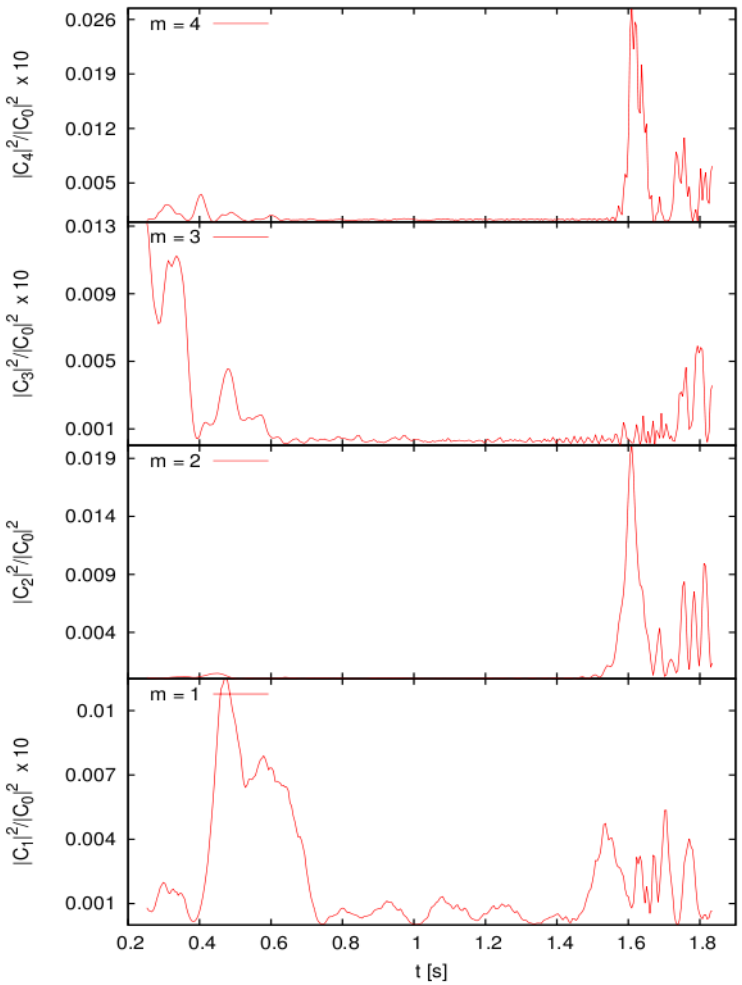

Fig. 18 Relative power $|c_m|^2 = |C_m|^2/|C_0|^2$ ($m = 1, 2, 3, 4$) for the azimuthal's distribution of mass Φ_M Fourier transform of $\beta 2.6$ model ($|c_m|^2$ values are scaled for modes $m = 1$, 3 and 4).

- Intense variations on $\dot{M}$ and L_c happen at the same time.
- The relative power $|c_2|^2$ has an intense peak ($\gtrsim 10$ times) at $t = 1.6$ where intense variations on $\dot{M}$ and L_c start.
- Intense structure formation $\rightarrow$ variations on L_c and $\dot{M}$

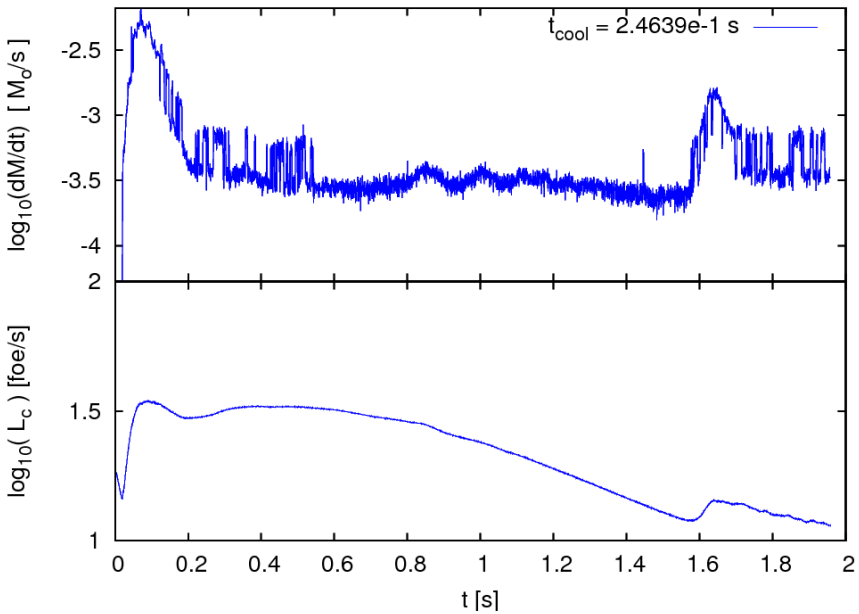

Fig. 19 Mass accretion and energy loss rates (top panel and bottom panel respectively).

$\beta 2.6$ Model

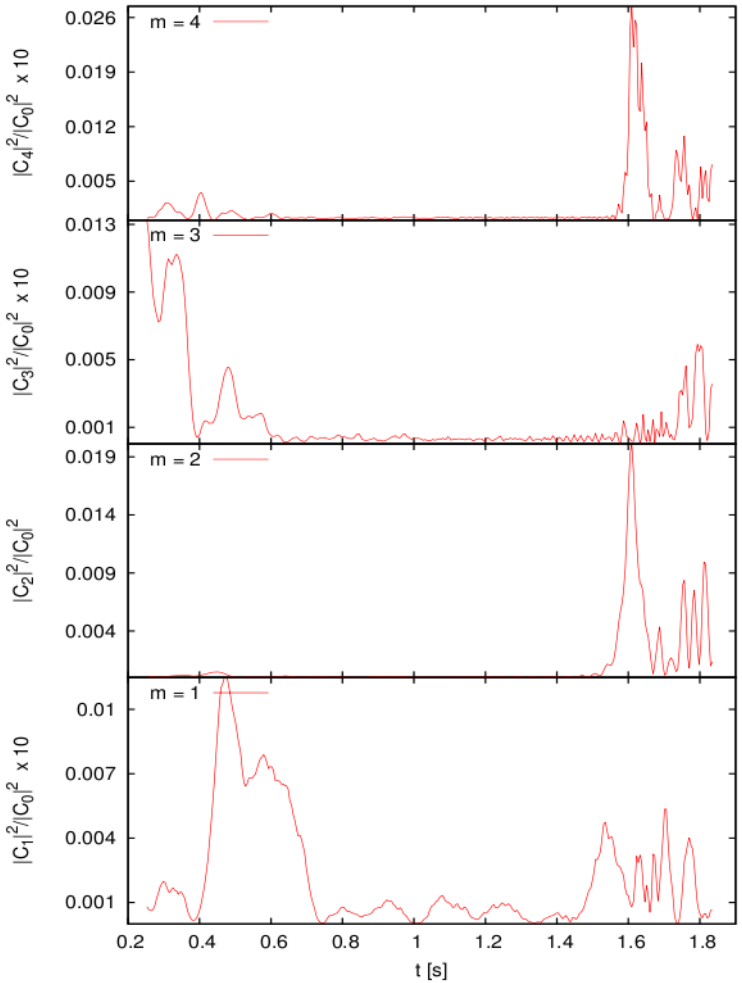

Fig. 18 Relative power $|c_m|^2 = |C_m|^2/|C_0|^2$ ($m = 1, 2, 3, 4$) for the azimuthal's distribution of mass Φ_M Fourier transform of $\beta 2.6$ model ($|c_m|^2$ values are scaled for modes $m = 1, 3$ and 4).

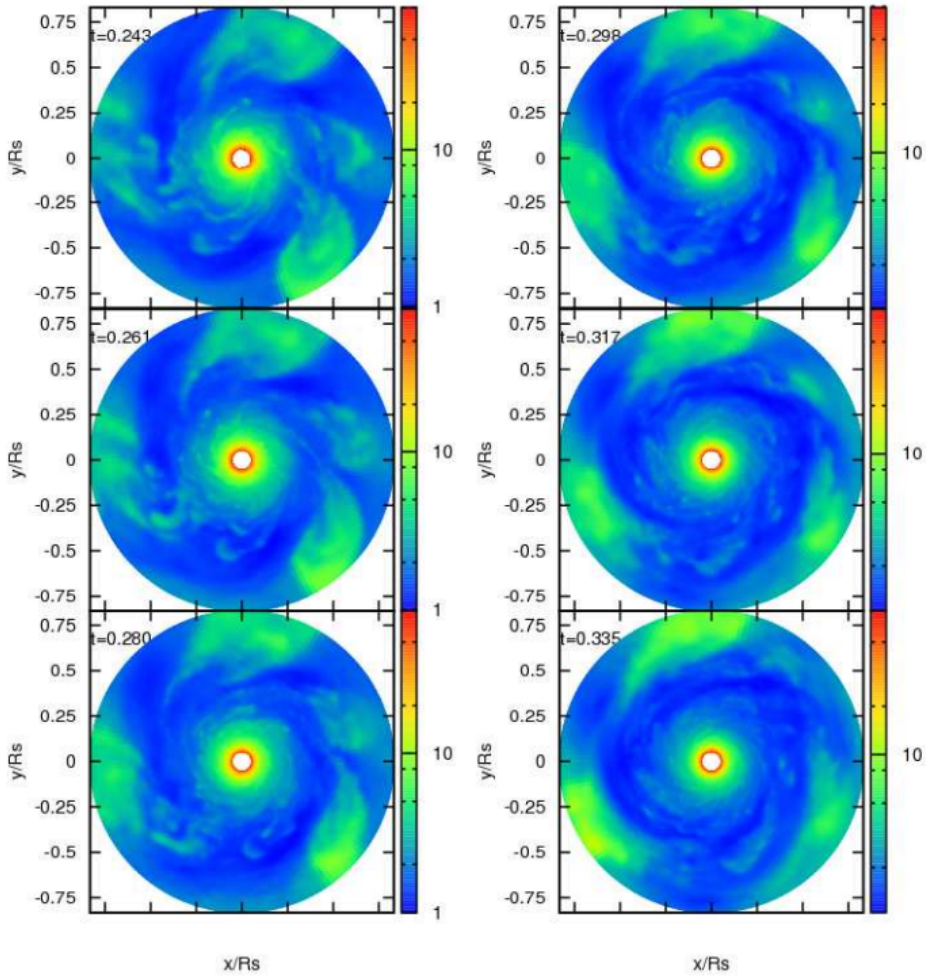

Fig. 20 Evolution of the Toomre parameter Q for the $\beta 2.6$ model at times $\simeq 0.2$ s. There is noticeable structure repeating every $2\pi/3$ radians but the lowest Toomre parameter (blue regions) have $Q \gtrsim 1$.

$\beta 2.6$ Model

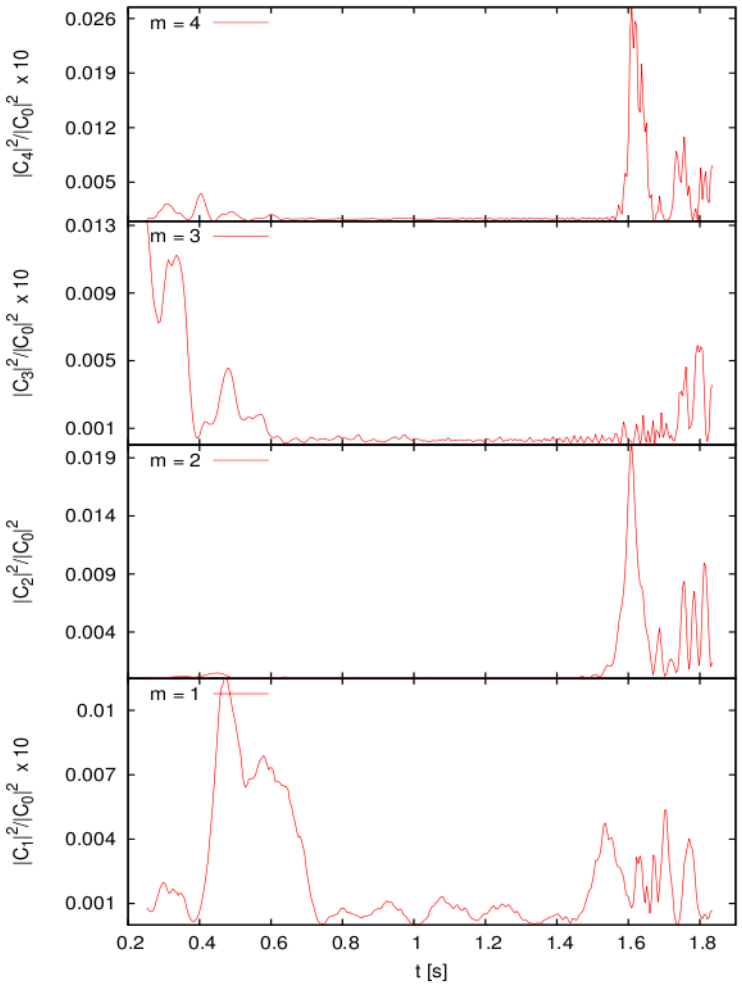

Fig. 18 Relative power $|c_m|^2 = |C_m|^2/|C_0|^2$ ($m = 1, 2, 3, 4$) for the azimuthal's distribution of mass Φ_M Fourier transform of $\beta 2.6$ model ($|c_m|^2$ values are scaled for modes $m = 1$, 3 and 4).

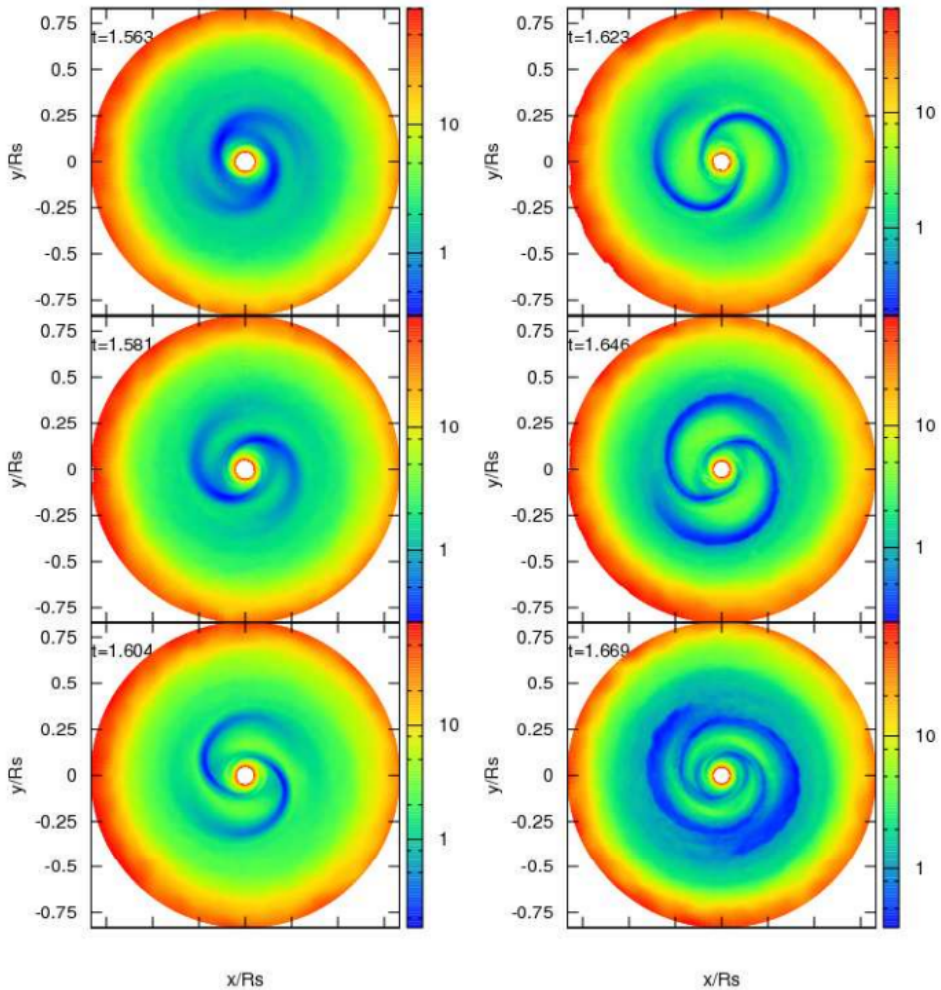

Fig. 21 Evolution of the Toomre parameter Q for the $\beta 2.6$ model at times $\simeq 1.6$ s. The two spiral arms with $Q < 1$ remain intense over ~ 0.1 s.

$\beta 1.3$ Model, $t_{cool} = 0.123$ s

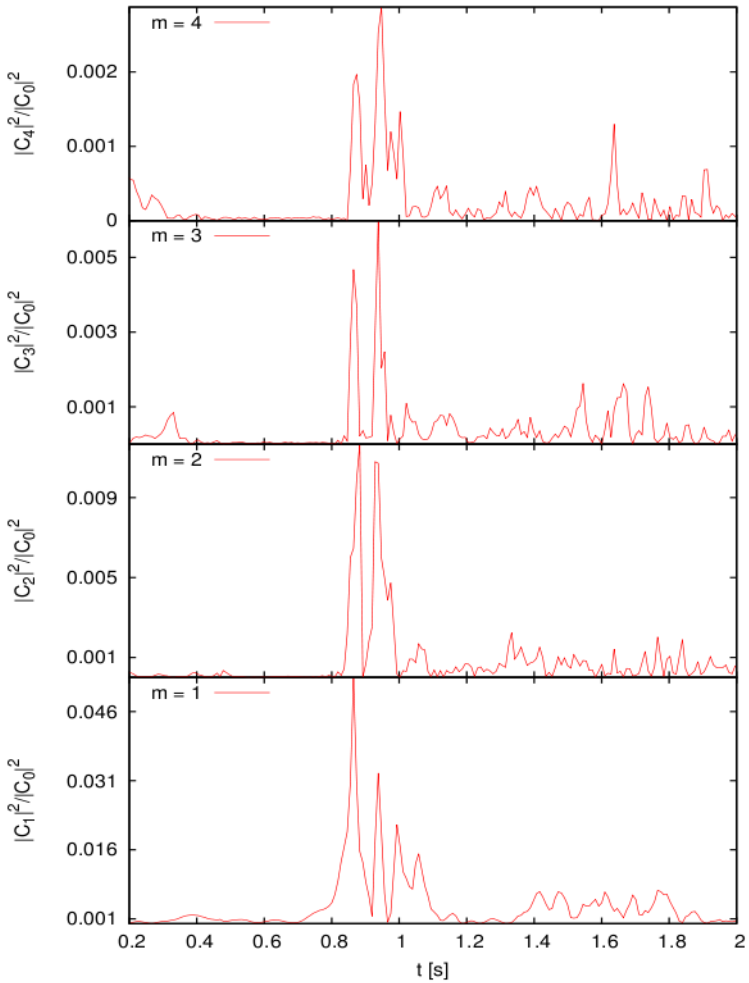

Fig. 22 Relative power $|c_m|^2$ ($m = 1, 2, 3, 4$) for the azimuthal's distribution of mass Φ_M Fourier transform of $\beta 1.3$ model.

- Intense variations on $\dot{M}$ and L_c happen at the same time.
- The relative power $|c_1|^2$ has the most intense peaks at $t \simeq 0.9$ s where intense variations on $\dot{M}$ and L_c start.
- Increasing cooling efficiency $\rightarrow$ earlier structure formation

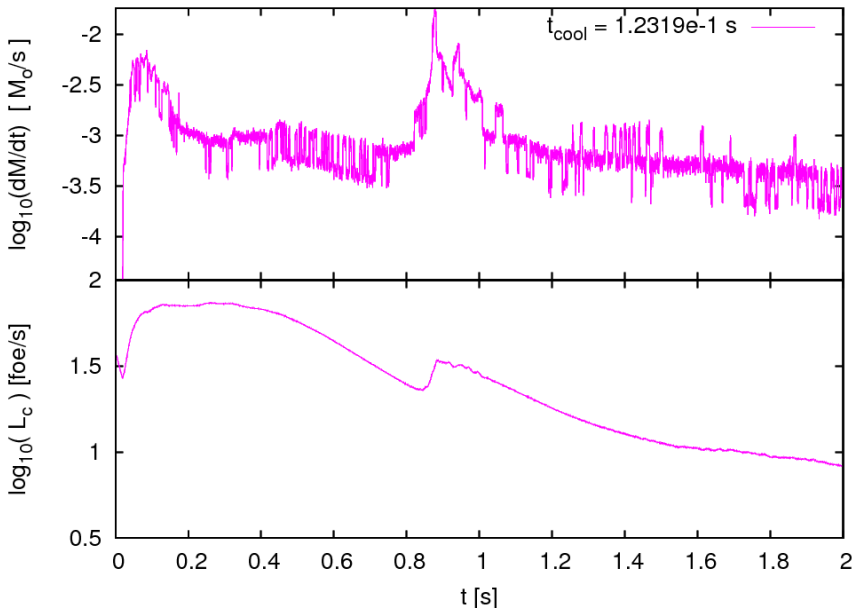

Fig. 23 Mass accretion and energy loss rates for $\beta 1.3$ model. (Top and bottom panel respectively).

$\beta 1.3$ Model, $t_{cool} = 0.123$ s

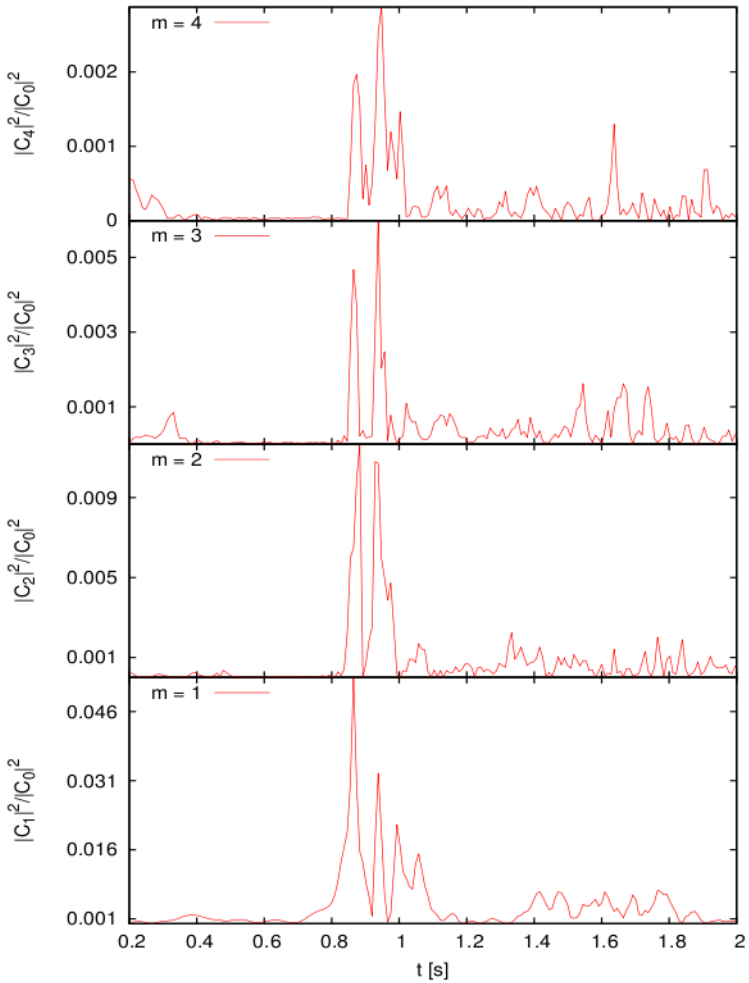

Fig. 22 Relative power $|c_m|^2$ $(m = 1, 2, 3, 4)$ for the azimuthal's distribution of mass Φ_M Fourier transform of $\beta 1.3$ model.

- Intense variations on $\dot{M}$ and L_c happen at the same time.
- The relative power $|c_1|^2$ has the most intense peaks at $t \simeq 0.9$ s where intense variations on $\dot{M}$ and L_c start.
- Increasing cooling efficiency $\rightarrow$ earlier structure formation

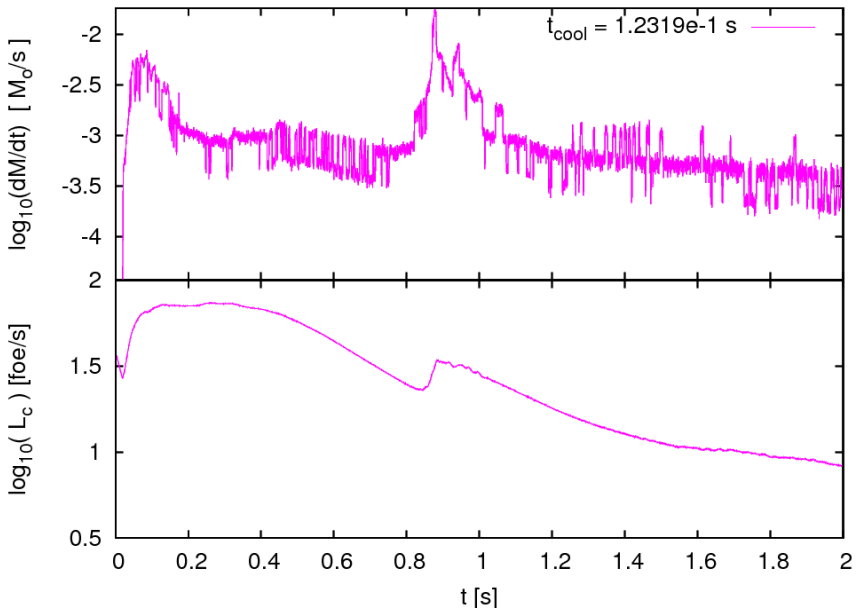

Fig. 23 Mass accretion and energy loss rates for $\beta 1.3$ model. (Top and bottom panel respectively).

$\beta 1.3$ Model

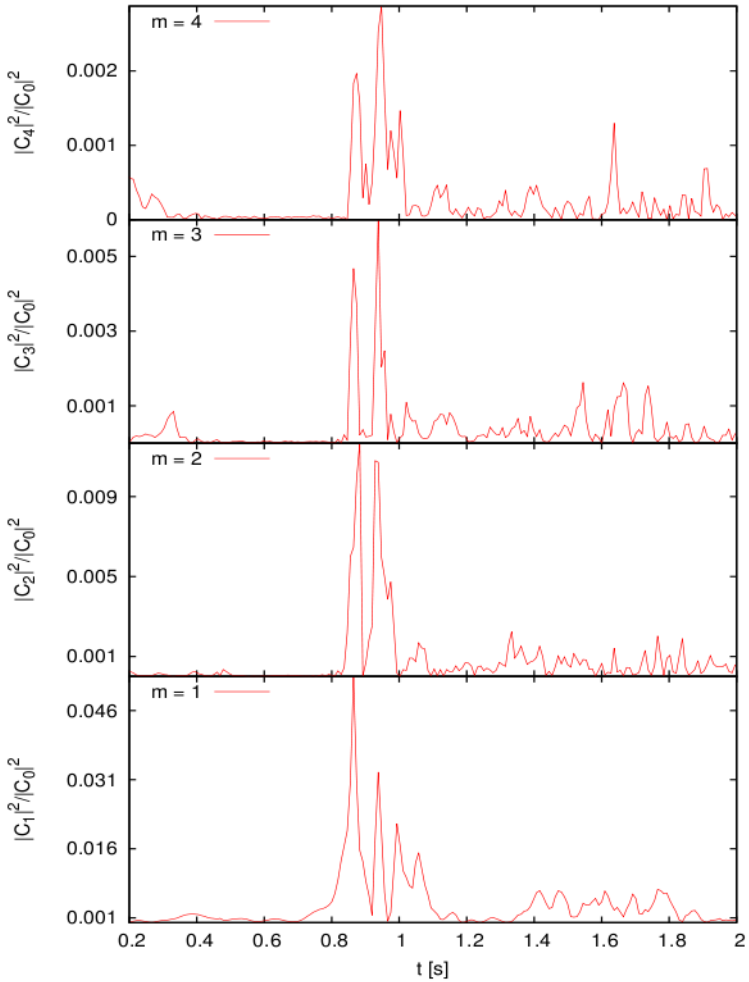

Fig. 22 Relative power $|c_m|^2$ $(m = 1, 2, 3, 4)$ for the azimuthal's distribution of mass Φ_M Fourier transform of $\beta 1.3$ model.

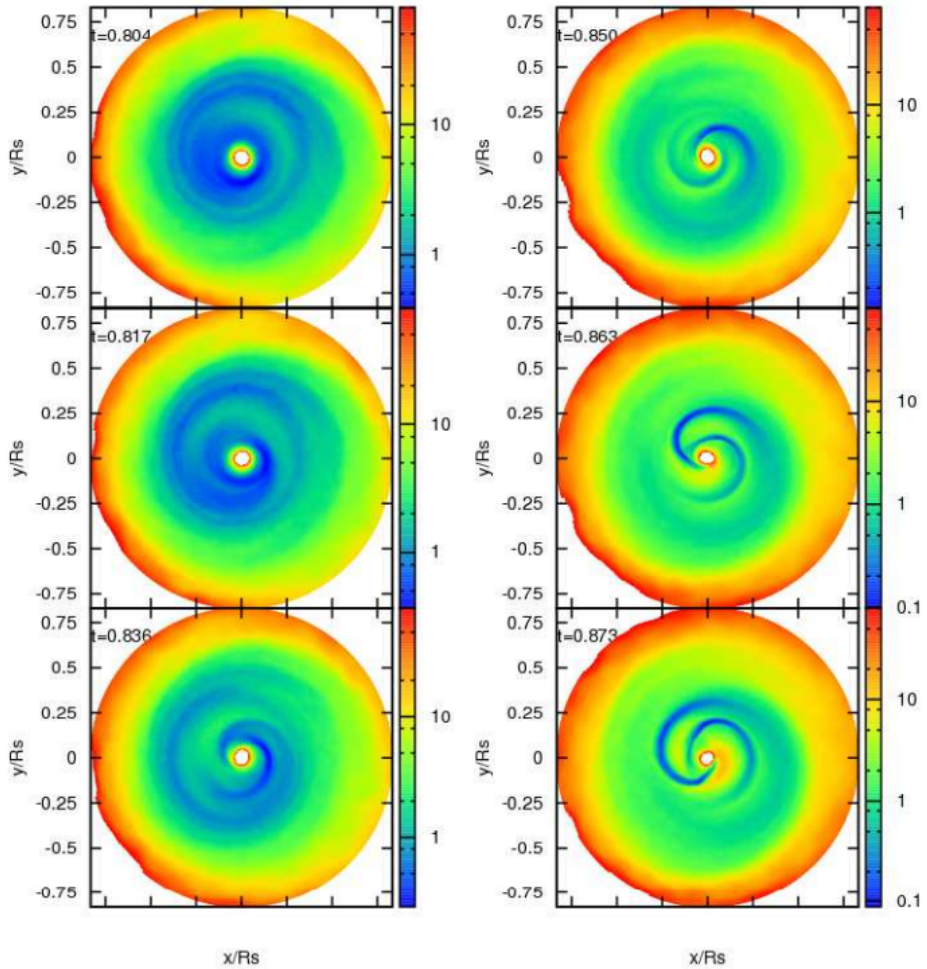

Fig. 24 Evolution of the Toomre parameter Q for the $\beta 1.3$ model at times $\simeq 0.9$ s. Deep blue regions have $Q < 0.1$. There is noticeable spiral structure and clumps at the unstable regions.

$\beta 1.3$ Model

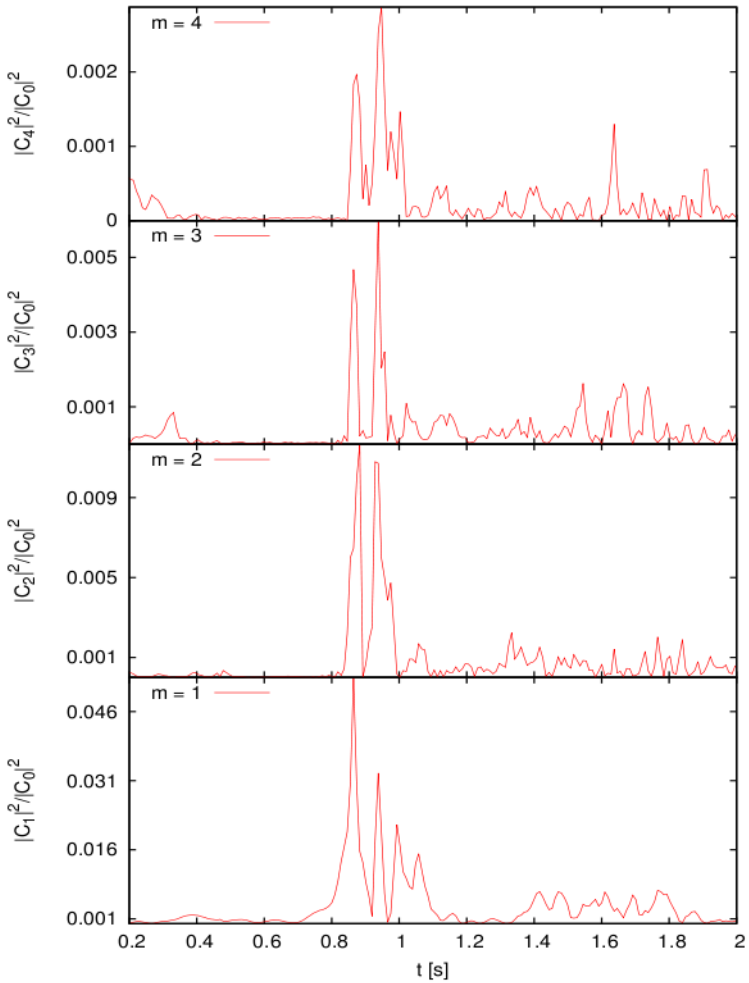

Fig. 22 Relative power $|c_m|^2$ ($m = 1, 2, 3, 4$) for the azimuthal's distribution of mass Φ_M Fourier transform of $\beta 1.3$ model.

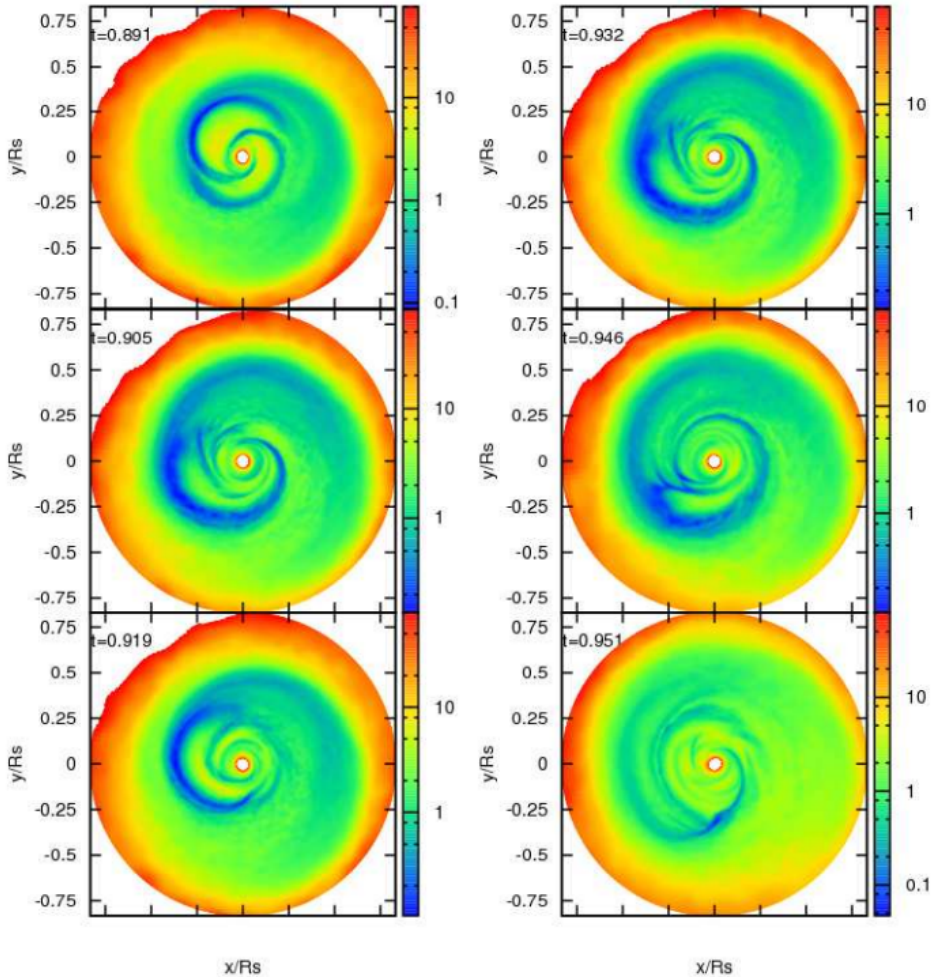

Fig. 25 Evolution of the Toomre parameter Q for the $\beta 1.3$ model at times $\simeq$ 1 s. Deep blue regions have $Q < 0.1$. There is noticeable spiral structure and clumps at the unstable regions.

$\beta 1.3$ Model

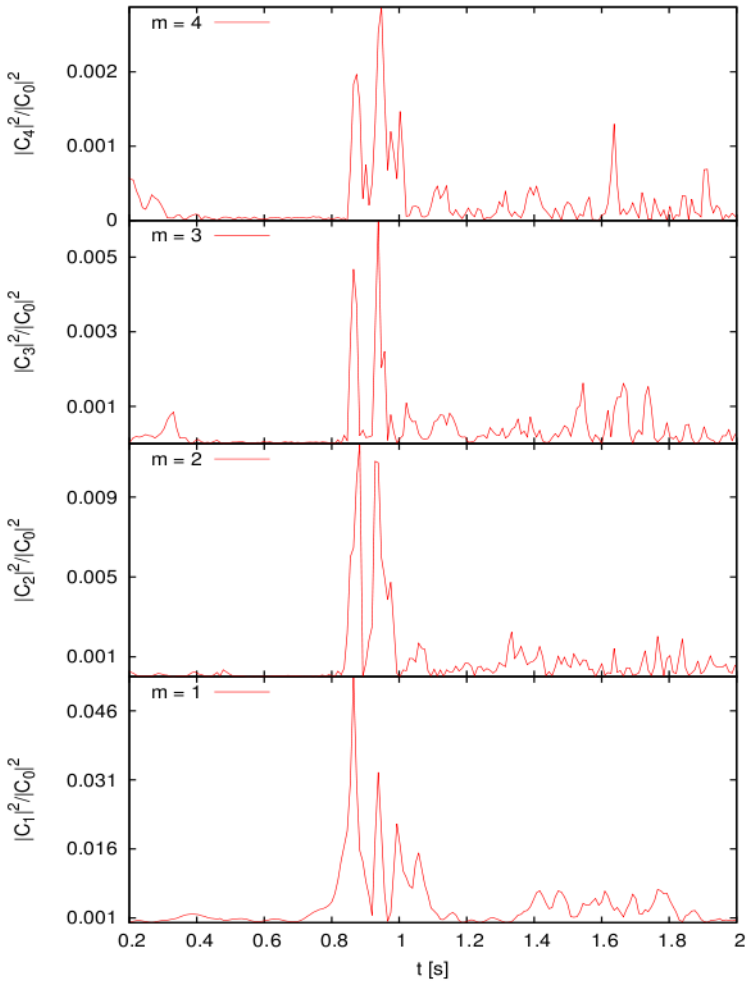

Fig. 22 Relative power $|c_m|^2$ ($m = 1, 2, 3, 4$) for the azimuthal's distribution of mass Φ_M Fourier transform of $\beta 1.3$ model.

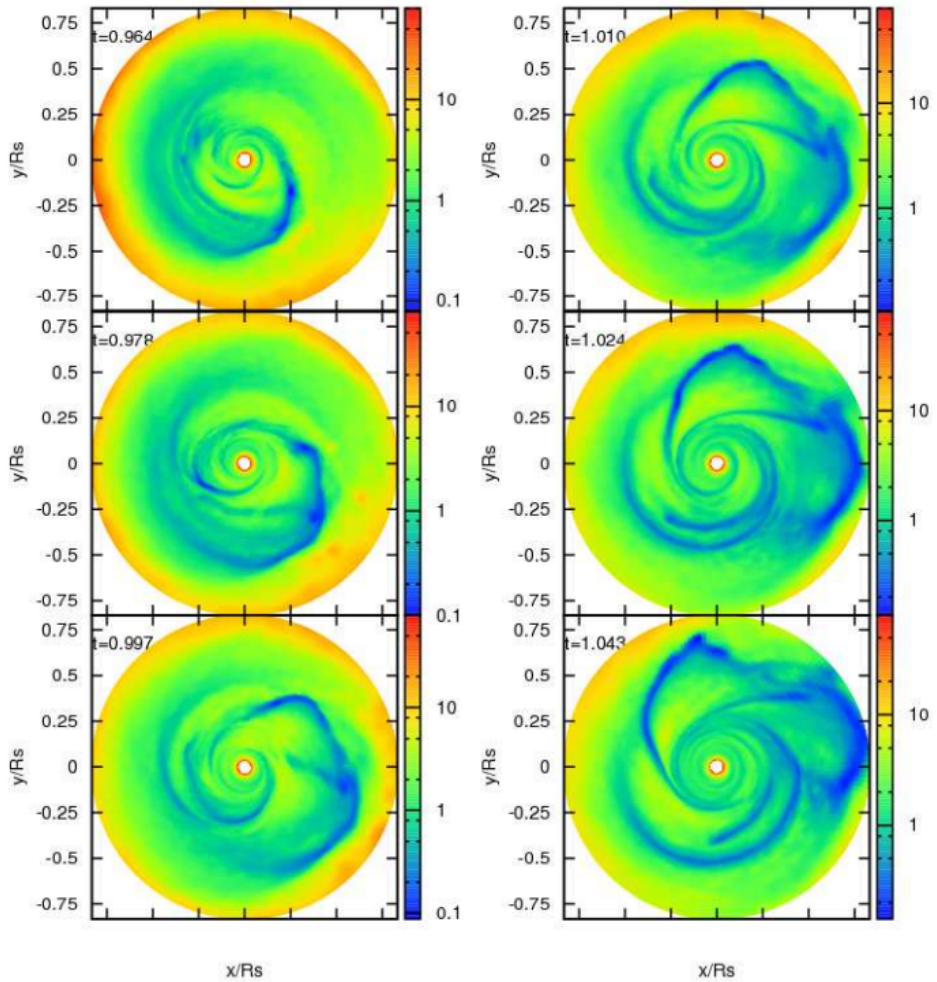

Fig. 26 Evolution of the Toomre parameter Q for the $\beta 1.3$ model at times $\simeq$ 1 s. Deep blue regions have $Q < 0.1$. There is noticeable spiral structure and clumps at the unstable regions.

$\beta 0.26$ Model, $t_{cool} = 0.0246$ s

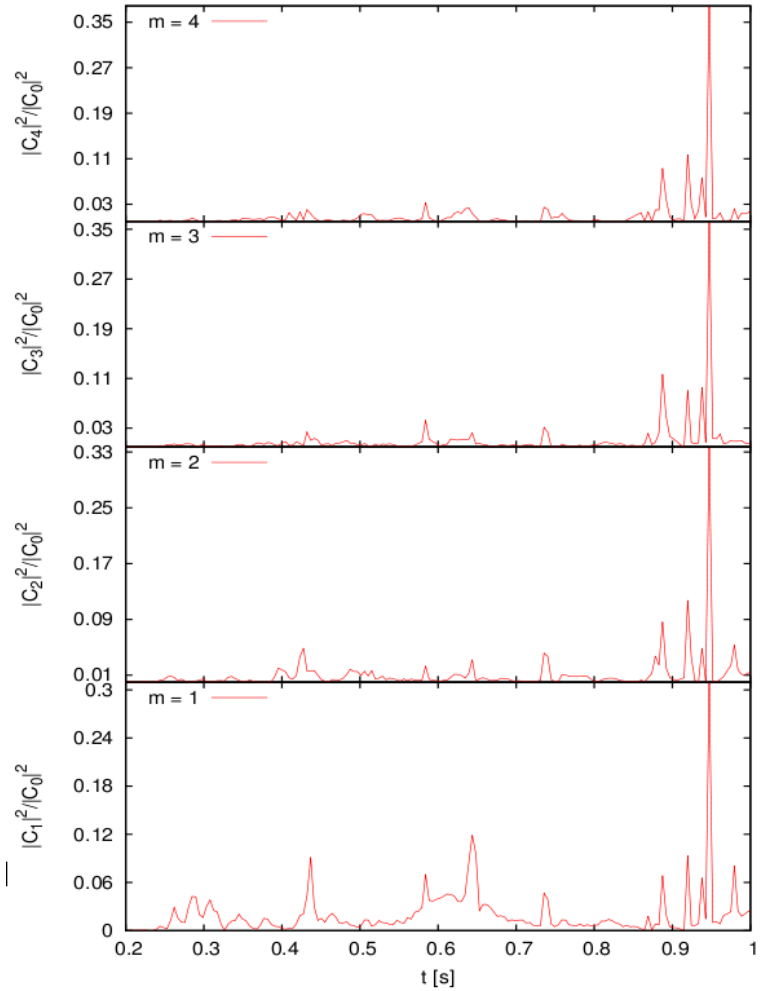

Fig. 27 Relative power $|c_m|^2 = |C_m|^2/|C_0|^2$ ($m = 1, 2, 3, 4$) for the azimuthal's distribution of mass Φ_M Fourier transform of $\beta 0.26$ model.

- Intense variations on $\dot{M}$ and L_c happen at the same time.
- The relative powers $|c_m|^2$ have an intense peak at $t \simeq 0.94$.
- Several episodes of intense variations on $\dot{M}$ and L_c, starting at earlier times

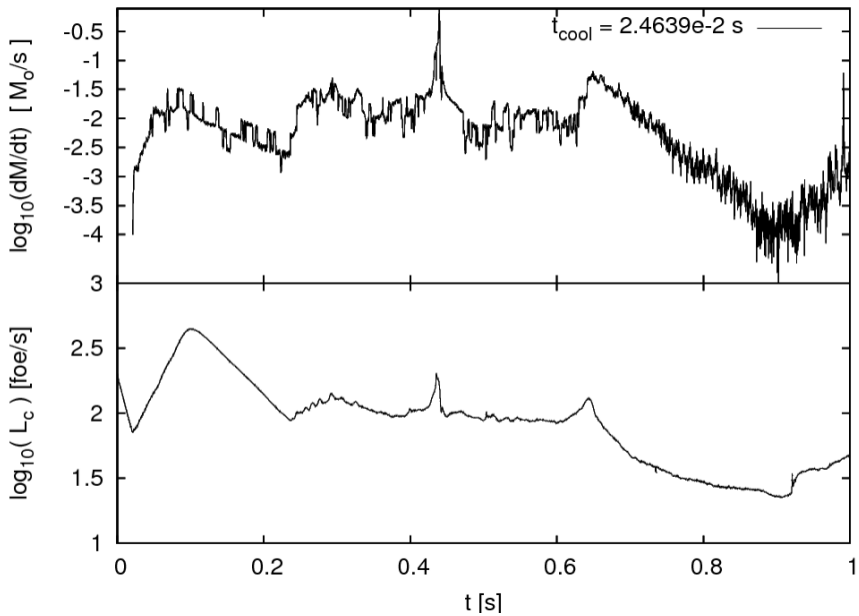

Fig. 28 Mass accretion and energy loss rates for $\beta 0.26$ model. (Top and bottom panel respectively)

$\beta 0.26$ Model, $t_{cool} = 0.0246$ s

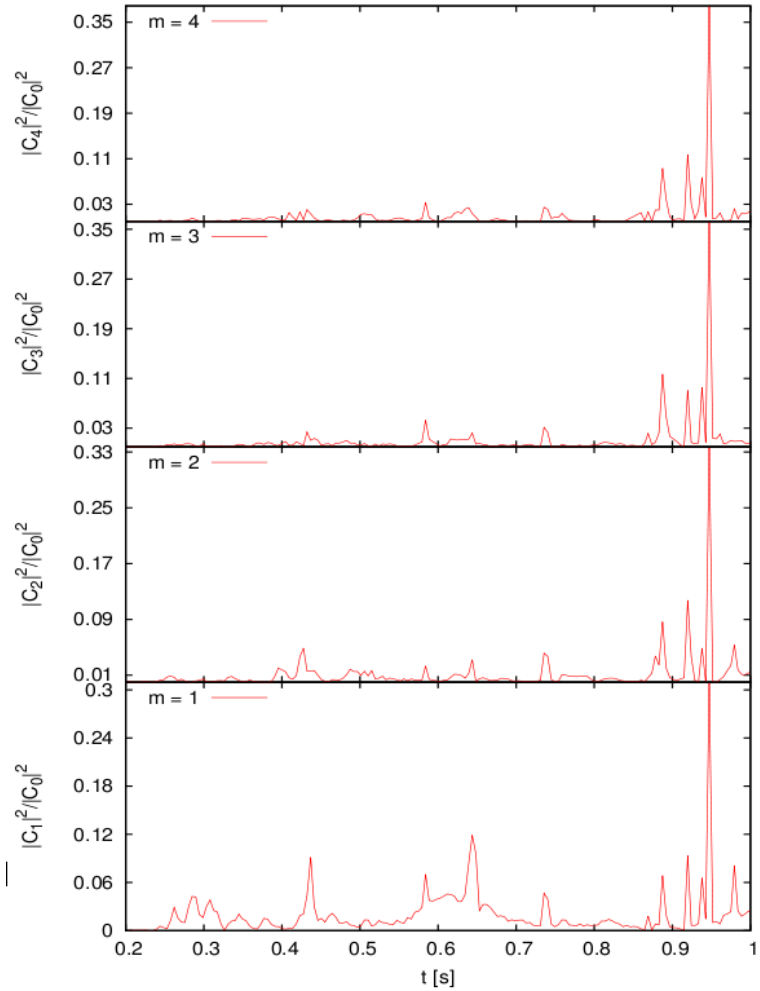

Fig. 27 Relative power $|c_m|^2 = |C_m|^2/|C_0|^2$ ($m = 1, 2, 3, 4$) for the azimuthal's distribution of mass Φ_M Fourier transform of $\beta 0.26$ model.

- Intense variations on $\dot{M}$ and L_c happen at the same time.
- The relative powers $|c_m|^2$ have an intense peak at $t \simeq 0.94$.
- Several episodes of intense variations on $\dot{M}$ and L_c, starting at earlier times

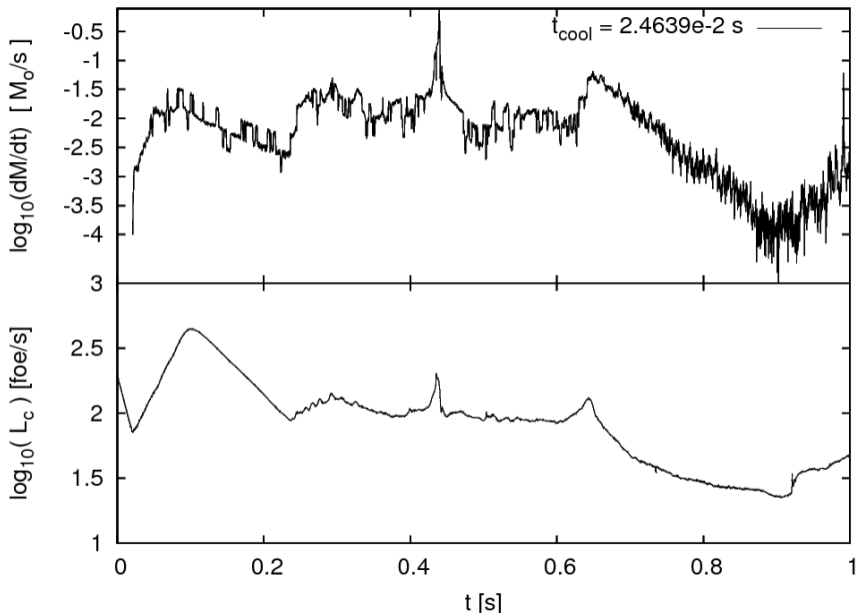

Fig. 28 Mass accretion and energy loss rates for $\beta 0.26$ model. (Top and bottom panel respectively)

$\beta 0.26$ Model

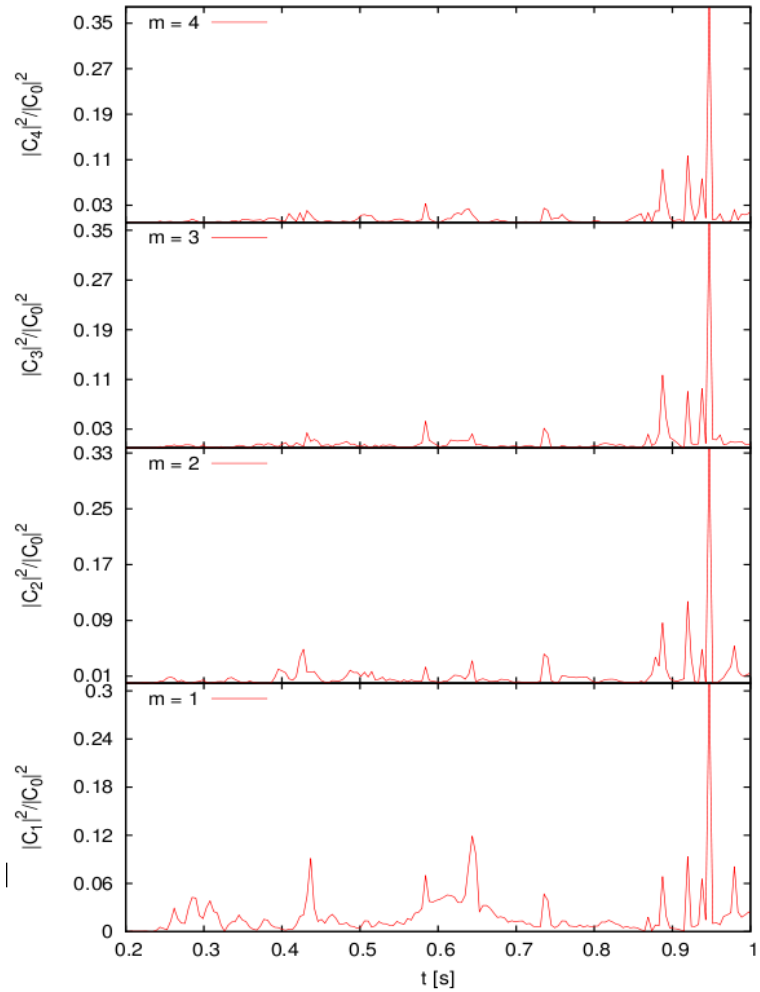

Fig. 27 Relative power $|c_m|^2 = |C_m|^2/|C_0|^2$ $(m = 1, 2, 3, 4)$ for the azimuthal's distribution of mass Φ_M Fourier transform of $\beta 0.26$ model.

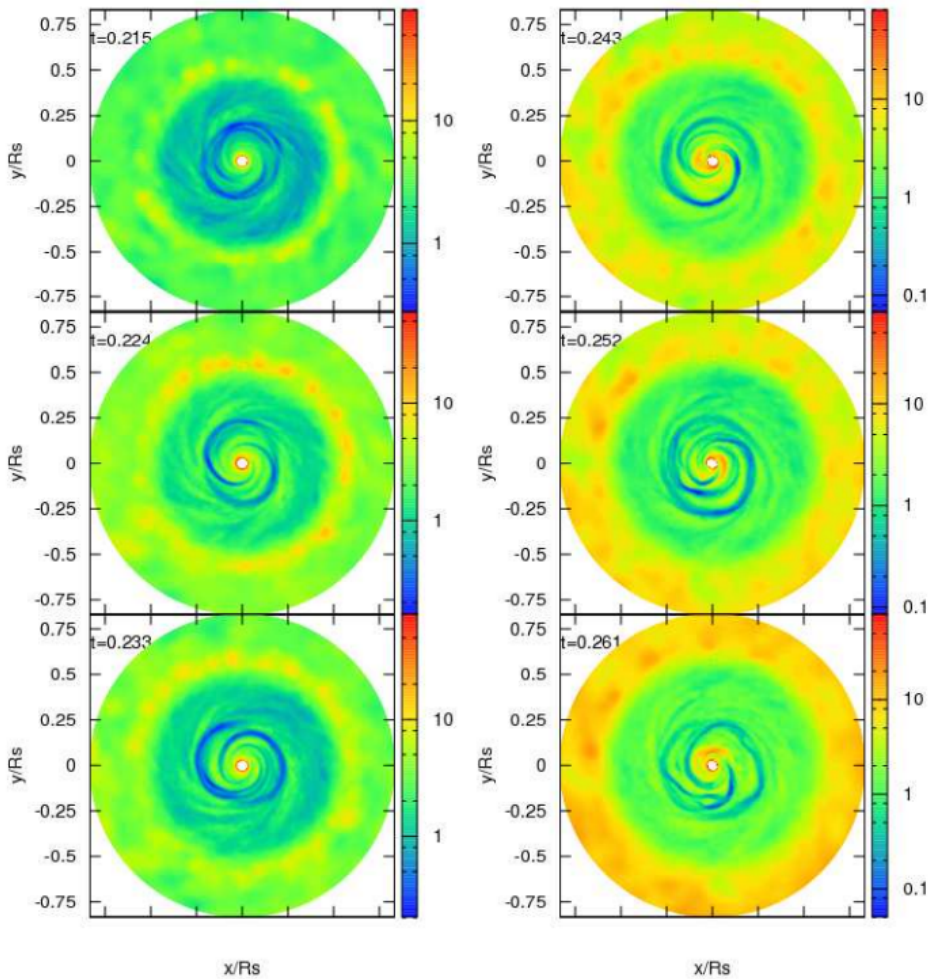

Fig. 29 Evolution of the Toomre parameter Q for the $\beta 0.26$ model at times $\simeq 0.2$ s. Deep blue regions have $Q \lesssim 0.1$. There are noticeable spiral arms and clumps formed at the most unstable regions.

$\beta 0.26$ Model

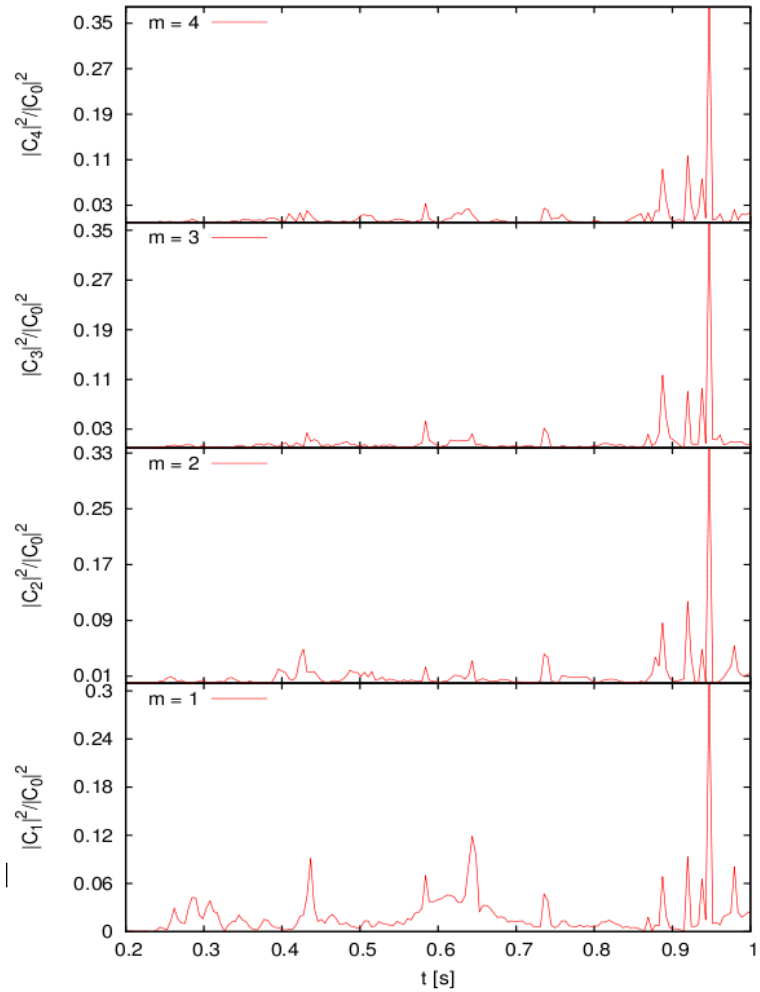

Fig. 27 Relative power $|c_m|^2 = |C_m|^2/|C_0|^2$ $(m = 1, 2, 3, 4)$ for the azimuthal's distribution of mass Φ_M Fourier transform of $\beta 0.26$ model.

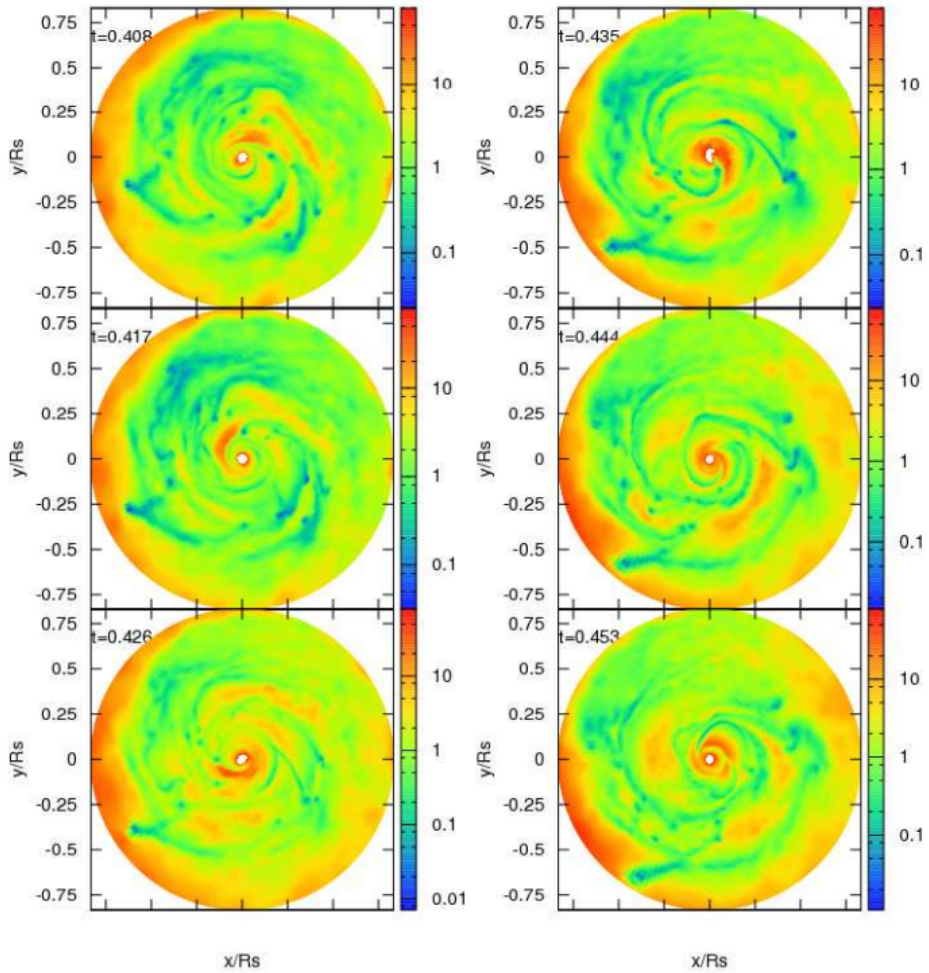

Fig. 30 Evolution of the Toomre parameter Q for the $\beta 0.26$ model at times $\simeq 0.4$ s. Deep blue regions have $Q \lesssim 0.01$. There are noticeable spiral arms and clumps formed at the most unstable regions.

$\beta 0.26$ Model

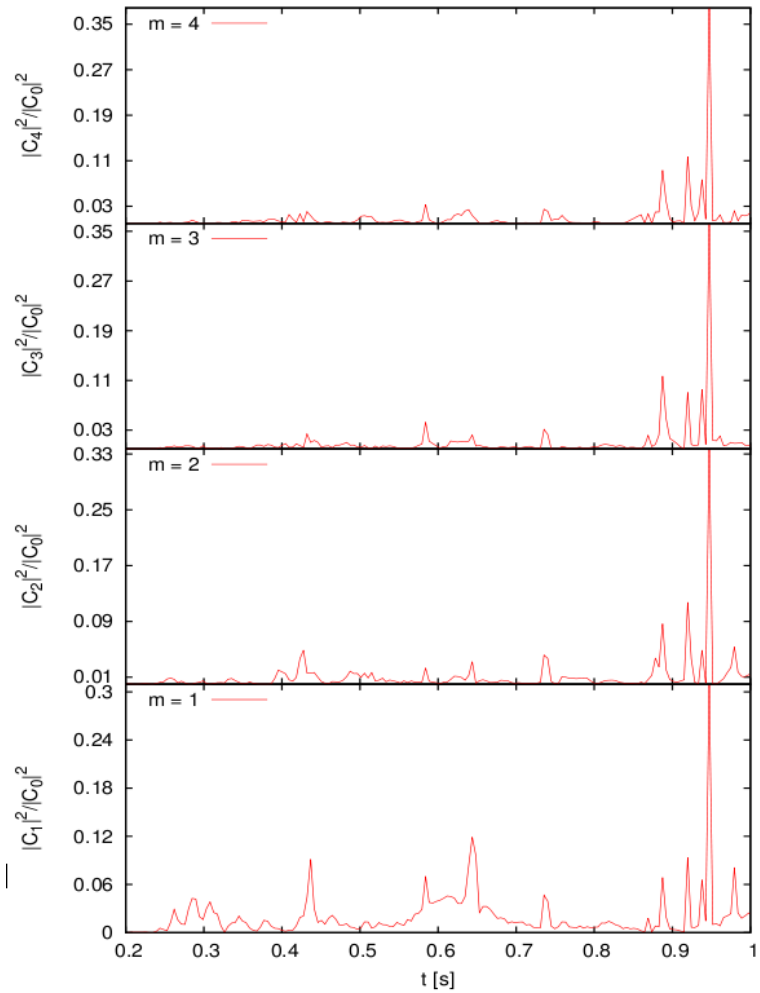

Fig. 27 Relative power $|c_m|^2 = |C_m|^2/|C_0|^2$ $(m = 1, 2, 3, 4)$ for the azimuthal's distribution of mass Φ_M Fourier transform of $\beta 0.26$ model.

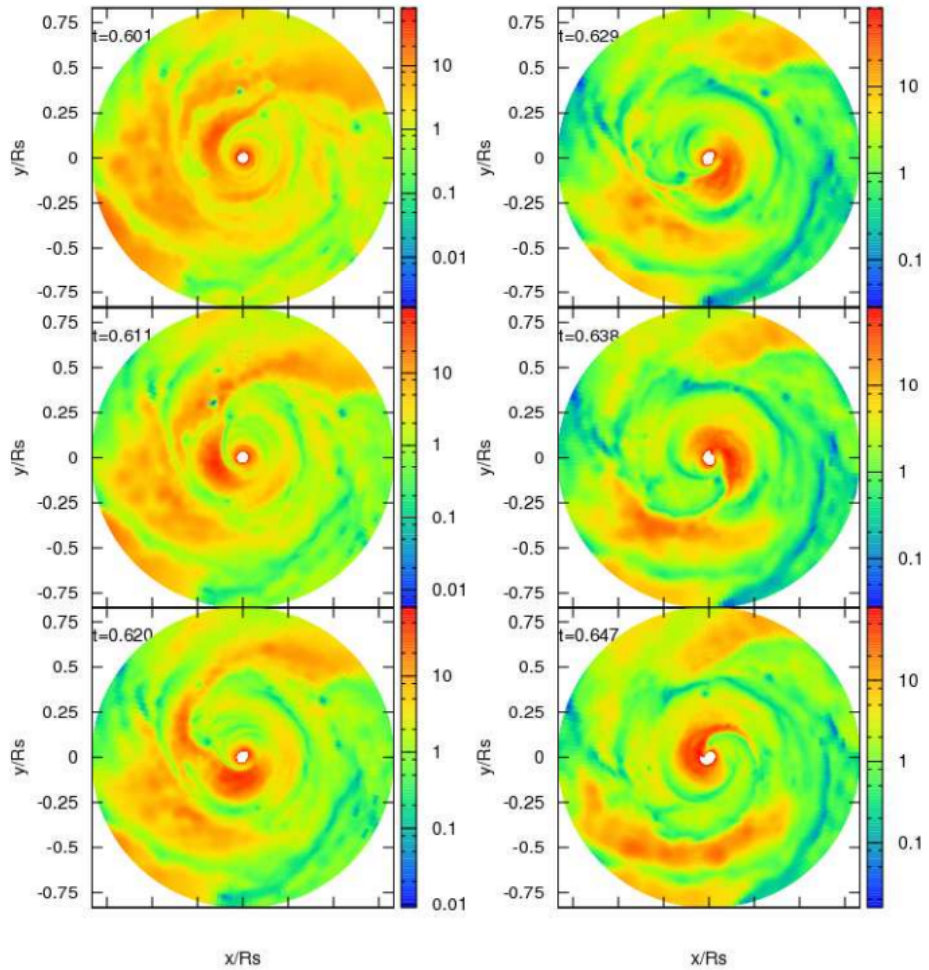

Fig. 31 Evolution of the Toomre parameter Q for the $\beta 0.26$ model at times $\simeq 0.6$ s. Deep blue regions have $Q \lesssim 0.01$. There are noticeable spiral arms and clumps formed at the most unstable regions.

$\beta 0.26$ Model

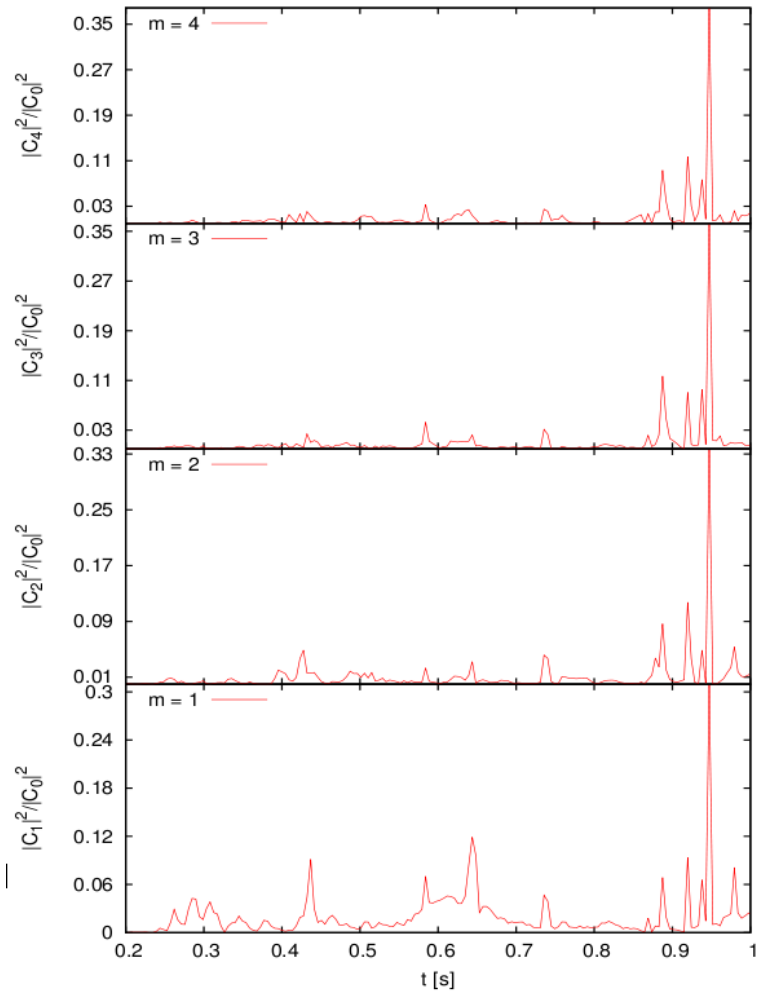

Fig. 27 Relative power $|c_m|^2 = |C_m|^2/|C_0|^2$ $(m = 1, 2, 3, 4)$ for the azimuthal's distribution of mass Φ_M Fourier transform of $\beta 0.26$ model.

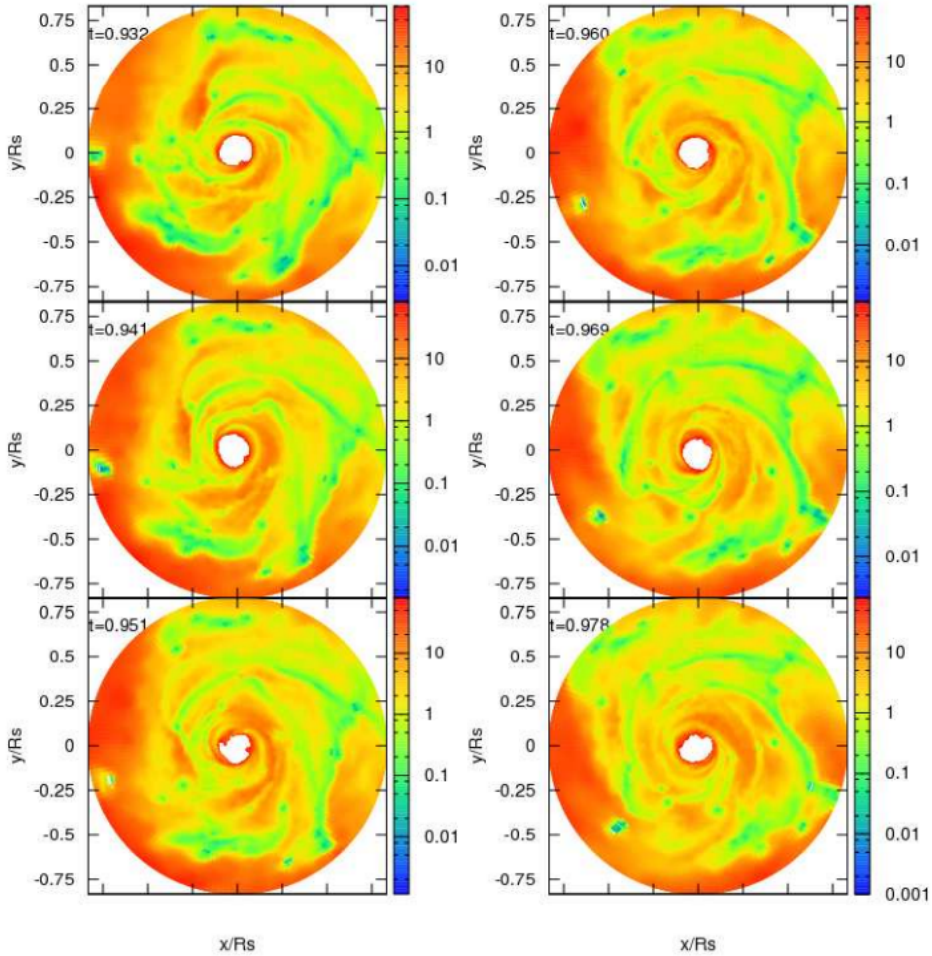

Fig. 32 Evolution of the Toomre parameter Q for the $\beta 0.26$ model at times $\simeq 0.9$ s. Deep blue regions have $Q \lesssim 0.01$. There are noticeable spiral arms and clumps formed at the most unstable regions.

$\beta 0.026$ Model, $t_{cool} = 0.00246$ s

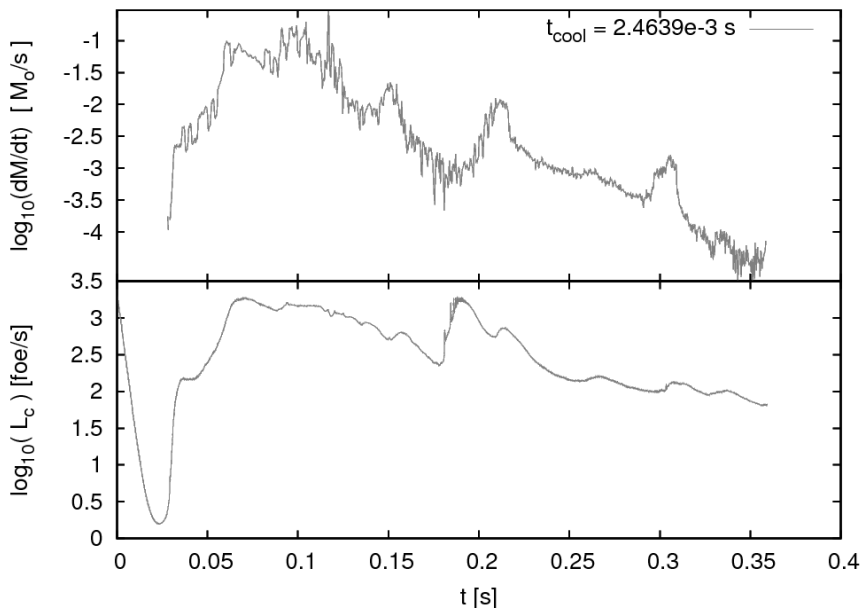

Fig. 34 Mass accretion and energy loss rates for $\beta 0.026$ model. (Top and bottom panel respectively).

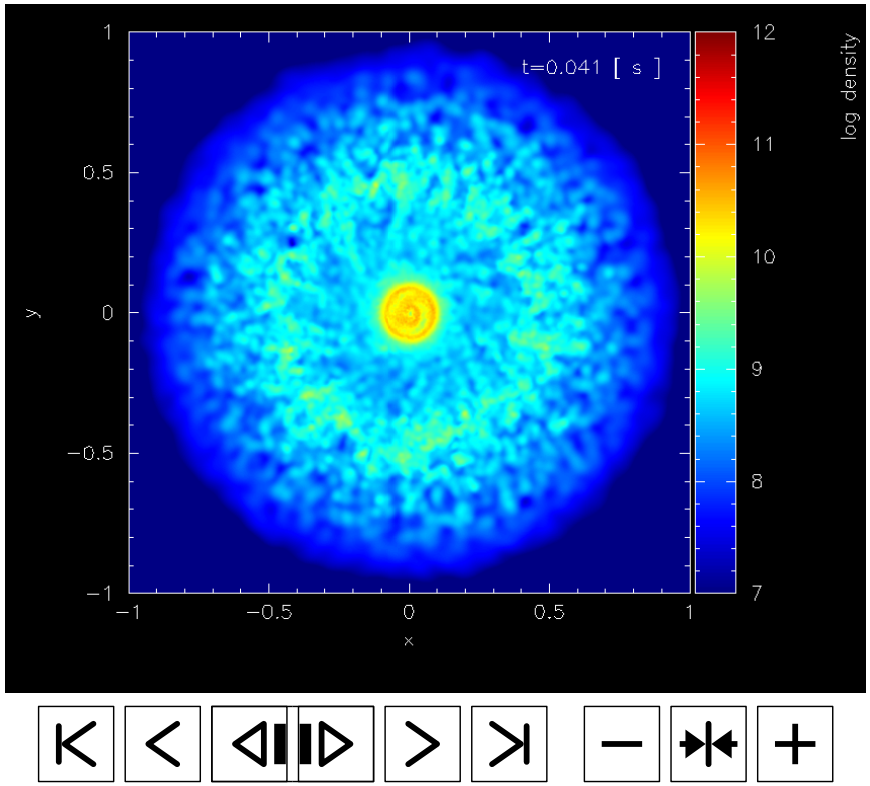

Summary

- Efficient cooling induces profuse and intense structure formation $\rightarrow$ L_c variability & symmetry break up altering BH-disk gravitational interaction $\rightarrow$ variation in $\dot{M}$.
  - For a massive enough accretion disk (as expected in the collapsar model) gravitational interactions between intense instabilities and the BH could change the BH position considerably.
- Duration & intensity of such variations depend on how collapsed the structures are. Structures with $Q \ll 1$ (such as clumps) will change $\dot{M}$ and L_c considerably if they come to close to the BH.
- When applying an adequate EOS and neutrino cooling, we expect to have intense variations in L_ν and $\dot{M}$ due to structure formation.

Thanks

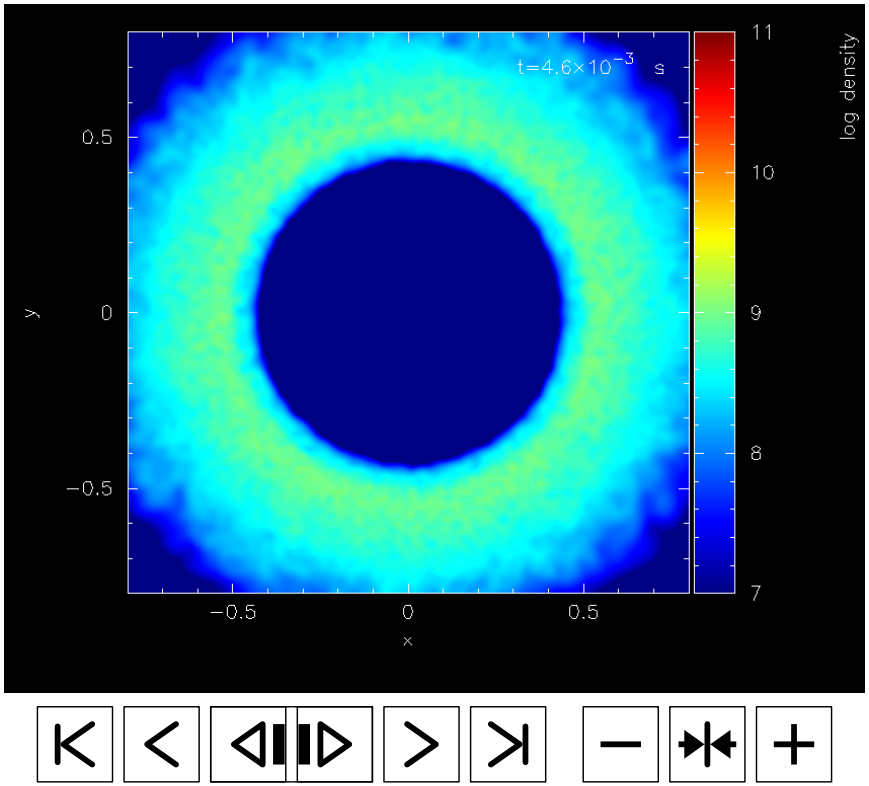

Referencias

N Gehrels, E. Ramirez-Ruiz y D.B. Fox *Gamma-Ray Bursts in the Swift Era.* Annu. Rev. Astron. Astrophys. 2009. 47:567–617

A.I. MacFadyen y S.E. Woosley *Collapsars: Gamma-Ray Bursts and explosions in "Failed Supernovae".* APJ, 524 : 262-289, 1999 October 10

S.E. Woosley *Gamma-Ray Bursts from Stellar Mass Accretion Disks Around Black Holes.* APJ, 405 : 273-277, 1993 March 1

S.E. Woosley y A. Heger *The Progenitor Stars of Gamma Ray Bursts.* APJ, 637 : 914-921, 2006 February 1

G. Rockefeller, C.L. Fryer y H. Li *Collapsars in Three Dimensions.* arXiv:astro-ph/0608028v1 1 Aug 2006

S.E. Woosley y T. Janka *The Physics of Core-Collapse Supernovae.* Nature physics Vol 1 December 2005

M.C. Begelman, E.M. Rossi y P.J. Armitage *Quasistars: Acreting Black Holes Inside Massive Envelopes.* 2008, MNRAS, 387, 1649

S.E. Woosley y J.S. Bloom *The Supernova-Gamma-Ray Bursts Connection.* Annu. Rev. Astron. Astrophys. 2006. 44:507–556

W.H. Lee, E. Ramirez Ruiz y D. Page *Dynamical Evolution of Neutrino-Cooled Accretion Disks: Detailed Microphysics, Lepton-Driven Convection, and Global Energetics* APJ, 632 : 421–437, 2005 October 10

Diego Lopez-Camara, William H. Lee y Enrico Ramirez-Ruiz *Gamma Ray Bursts and Supernova Signatures in Slowly Rotating Collasars* Accepted by APJ ArXiv:0808.0462v2 [astro-ph]

S.E. Woosley, A. Heger & T.A. Weaver, *The evolution and explotion of massive stars*.Rev. Mod. Phys. (2002). 74:1015-1071